



HAL
open science

How do continents deform during mantle exhumation? Insights from the northern Iberia inverted paleo-passive margin, western Pyrenees (France).

Riccardo Asti, Yves Lagabrielle, Serge Fourcade, Benjamin Corre, Patrick
Monie

► To cite this version:

Riccardo Asti, Yves Lagabrielle, Serge Fourcade, Benjamin Corre, Patrick Monie. How do continents deform during mantle exhumation? Insights from the northern Iberia inverted paleo-passive margin, western Pyrenees (France).. *Tectonics*, 2019, 38 (5), pp.1666-1693. 10.1029/2018TC005428 . insu-02108893

HAL Id: insu-02108893

<https://insu.hal.science/insu-02108893>

Submitted on 3 Jul 2019

HAL is a multi-disciplinary open access archive for the deposit and dissemination of scientific research documents, whether they are published or not. The documents may come from teaching and research institutions in France or abroad, or from public or private research centers.

L'archive ouverte pluridisciplinaire **HAL**, est destinée au dépôt et à la diffusion de documents scientifiques de niveau recherche, publiés ou non, émanant des établissements d'enseignement et de recherche français ou étrangers, des laboratoires publics ou privés.

Tectonics

RESEARCH ARTICLE

10.1029/2018TC005428

Key Points:

- Thin lenses of ductilely deformed pre-Silurian crustal basement rocks are welded on the exhumed mantle in the distal passive margin domain
- Temperatures of the late Albian ductile deformation in the pre-Silurian crustal basement rocks are in the range of ~350–450 °C
- The lower granulitic crust is not exhumed together with the mantle in the distal domain of the passive margin

Correspondence to:

R. Asti,
riccardo.asti@univ-rennes1.fr

Citation:

Asti, R., Lagabrielle, Y., Fourcade, S., Corre, B., & Monié, P. (2019). How do continents deform during mantle exhumation? Insights from the northern Iberia inverted paleopassive margin, western Pyrenees (France). *Tectonics*, 38, 1666–1693. <https://doi.org/10.1029/2018TC005428>

Received 20 NOV 2018

Accepted 6 APR 2019

Accepted article online 17 APR 2019

Published online 16 MAY 2019

How Do Continents Deform During Mantle Exhumation? Insights From the Northern Iberia Inverted Paleopassive Margin, Western Pyrenees (France)

Riccardo Asti¹ , Yves Lagabrielle¹, Serge Fourcade¹, Benjamin Corre¹, and Patrick Monié²

¹University of Rennes, CNRS, Géosciences Rennes-UMR 6118, Rennes, France, ²Géosciences Montpellier, Université Montpellier, UMR 5243 CNRS/INSU, Montpellier Cedex, France

Abstract Extreme crustal thinning associated with subcontinental mantle exhumation characterizes the distal domain of some current, magma-poor continental passive margins. Since these domains lie at abyssal depths and are hardly accessible, their internal structure and the finite strain of the stretched crust are not directly observed and are only inferred. A detailed field study was conducted on exceptionally preserved Cretaceous distal margin analogs in two key areas of the western Pyrenees (North Pyrenean Zone): the Urdach and Saraillé ultramafic massifs in the Chaînons Béarnais range. A tight sampling allowed us to characterize the conditions of the ductile deformation of the continental crust exhumed together with the mantle. New ⁴⁰Ar/³⁹Ar dating on muscovite constrains the timing of the last deformation of the continental crust in relation with mantle exhumation to the late Albian. We propose a new reconstruction for the distal part of the North Iberian paleopassive margin based on the following constraints: (i) post-Silurian Paleozoic rocks are never found in the distal domain; (ii) lower crustal levels are not found in the exhumed crustal units; (iii) extension in the pre-Silurian series is accomplished by lenticular deformation and pervasive ductile flattening through anastomosing extensional mylonitic shear zones at temperatures of 350–450 °C; and (iv) at the final step of exhumation, only pre-Silurian crustal lenses remained welded on the exhumed mantle. Finally, we discuss the importance of the crustal structure inherited from previous Paleozoic and Mesozoic tectonic events and we state that mantle exhumation was partially achieved before the Cretaceous North Pyrenean rifting.

1. Introduction

Based on recent geophysical investigations around the world, the architecture of emblematic passive continental margins systematically appears composed of three distinct structural domains: the proximal, necking, and distal domains. Each margin domain is associated with specific lithospheric deformation processes finally resulting in the extreme thinning of the continental basement. It is now well established that the necking domain accommodates most of the change in the amount of extension between the proximal and the distal domain and that exhumation of the subcontinental lithospheric mantle frequently occurs in the distal domain (Peron-Pinvidic & Osmundsen, 2016). However, since continental margins lie at abyssal depths and are difficult to access, the finite state of strain and the mechanisms of deformation of the thinned to hyperthinned continental crust are not directly observed in the necking and distal domains of present-day passive margins and thus are only inferred.

Inverted necking and distal domains of paleopassive margins are preserved as internal tectonic units in several Cenozoic mountain belts such as the Alps (Mohn et al., 2012), the Pyrenees (Lagabrielle et al., 2010; Teixell et al., 2016), and the Zagros (Wrobel-Daveau et al., 2010). These domains have been recognized also in the Appalachian-Caledonian orogenic belt (Andersen et al., 2012; Chew & van Staal, 2014). Such field analogs represent unique geological laboratories that enable critical observations to constrain the mechanisms of crustal thinning and mantle exhumation during the formation of passive margins. The Pyrenean belt results from the collision of the southern European and northern Iberian passive continental margins that separated during a phase of transtensional deformation in the Albian-Cenomanian times. Shortening in the Pyrenees did not exceed 150 km but was sufficient to allow the distal portions of the inverted Iberia margin to be exhumed and uplifted and to be now exposed all along the northern flank of the belt in the North Pyrenean Zone (NPZ).

In this article, we provide new geological information from exceptionally preserved mantle and crustal remnants, belonging to the distal part of the North-Iberian paleopassive margin, exposed in the « Chaînons Béarnais » range of the western NPZ. Our focus is the deformation of the most distal remnants of the hyperthinned continental crust. Recent detailed reconstructions of the former margin architecture in this region point to a relatively short necking domain passing to a subsiding domain characterized by the presence of subcontinental peridotite bodies (Jammes et al., 2009; Lagabrielle et al., 2010; Masini et al., 2014; Teixell et al., 2016; Teixell et al., 2018; Tugend et al., 2014). We studied juxtaposed continental and ultramafic units exposed in two key areas: the Urdach and Saraillé massifs. These units preserve original geometrical relationships between them, allowing reconstruction of primary structures at the scale of the entire distal domain. A tight sampling of a great variety of Paleozoic crustal lithologies has been completed in units of massive crustal rocks as well as in tectonosedimentary breccia deposited over the exhumed ultramafic seafloor. Thin section studies provide details on the petrography, microstructure, and mineralogy of more than 90 samples. The aim is to release a representative image of the finite strain pattern of the hyperthinned crust and to determine the temperature conditions of the last stages of the mantle ascent close to the Earth surface. We discuss the density of discontinuous ductile mylonitic shear zones in the crust and the development of undulating detachment faults that separate less deformed crustal lenses. In addition, new $^{40}\text{Ar}/^{39}\text{Ar}$ dating on muscovite from deformed Variscan basement rocks enable us to constrain the timing of the last ductile extensional deformation and its relation with mantle exhumation. Finally, we discuss the importance of the crustal structure inherited from pre-Cretaceous (Variscan and Mesozoic) events on the style of mantle exhumation in the North-Pyrenean rift.

2. Geological Setting

2.1. The Pyrenees and the North Pyrenean Zone

The Pyrenees are an E-W trending, double-verging continental thrust-and-fold belt that developed in response to the collision between the margins of the northern Iberia and southern Europa plates during the Late Cretaceous-Cenozoic (Figure 1; Choukroune & ECORS team, 1989; Deramond et al., 1993; Muñoz, 1992; Roure & Choukroune, 1998; Teixell, 1998). All along the northern flank of the Pyrenees, in the NPZ, Triassic and Jurassic aborted rifting events preceded the development of Cretaceous rifts that resulted in crustal separation between Iberia and Europa and in the exhumation of subcontinental lithospheric mantle in the rift axis (Puigdefabregas & Souquet, 1986; Vergés & Garcia-Senz, 2001; Vielzeuf & Kornprobst, 1984). Continental rifting in the future Pyrenean belt was coeval with oceanic spreading in the Bay of Biscay between Chron M0 and A330 (~125–83 Ma), in relation with the counterclockwise rotation of Iberia relative to Europe (Choukroune & Mattauer, 1978; Le Pichon et al., 1970; Olivet, 1996; Sibuet et al., 2004). Two main plate kinematic models exist for the Cretaceous movements of the Iberian plate and the relative opening of the Bay of Biscay: (i) a model implying the opening of the Bay in a left-lateral transtensional setting (e.g., Le Pichon et al., 1970; Olivet, 1996) and (ii) a model claiming for a scissor-type opening of the Bay (Sibuet et al., 2004; Srivastava et al., 2000; Vissers & Meijer, 2012). The second model implies convergence in the Pyrenean realm during the opening of the Bay of Biscay and is inconsistent with field observations in the Pyrenees (e.g., Nirrengarten et al., 2018, and references therein).

The NPZ is well known for the occurrence of numerous small-sized bodies of subcontinental mantle rocks, mostly lherzolites, scattered within Mesozoic sedimentary formations, often in contact with Paleozoic rocks (Fabriès et al., 1991; Fabriès et al., 1998; Monchoux, 1970). Exhumation of subcontinental mantle following extreme continental thinning during the mid-Cretaceous rifting event has been proposed as a general mechanism accounting for the presence of such ultramafic material within the NPZ (Jammes et al., 2009; Lagabrielle & Bodinier, 2008). In addition, the prerift Mesozoic sequences of the NPZ underwent low-pressure-high-temperature deformation that developed in relation with thinning of the continental basement (Golberg & Leyrelop, 1990). Chronological and geological data enhance a correlation between the distribution of the highest paleotemperatures in the prerift sedimentary cover and the loci of extreme crustal stretching (Clerc et al., 2015). This correlation led Clerc and Lagabrielle (2014) to propose a mechanism of rifting involving the boudinage of the continental crust and the lateral extraction of the Paleozoic basement under a mobile Mesozoic prerift cover decoupled on thick Upper Triassic (Keuper) clays and evaporites layers. As a result, the subcontinental peridotites generally directly underlie the Mesozoic prerift metasediments. In the NPZ, Albian-Cenomanian flysch sequences were deposited synchronously with the synmetamorphic ductile

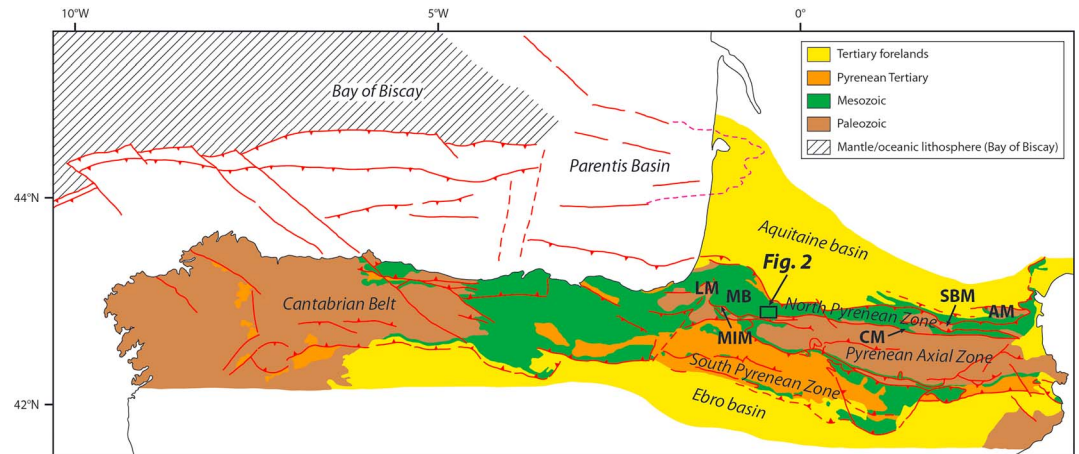


Figure 1. Synthetic tectonic map of the Pyrenean-Cantabrian chain showing the main tectonic structures (redrawn and modified after Teixell et al., 2018). In the black rectangle the location of the study area. Abbreviations: AM = Agly massif; CM = Castillon massif; LM = Labourd massif; MB = Mauléon Basin; MIM = Mendibelza and Igounze massifs; SBM = Saint-Barthélémy massif.

deformation of the prerift sequences and acted as a blanket allowing temperature increase in the mobile prerift cover (e.g., Lagabrielle et al., 2016). Continuous spreading of the basin floor triggered exhumation of the metamorphic, ductilely sheared prerift cover itself (Clerc et al., 2016).

2.2. The Chaînons Béarnais Range and Its Mantle Bodies (Western NPZ)

The Mesozoic prerift and synrift sediments of the western NPZ are exposed in the Chaînons Béarnais range, north of the western termination of the Axial Zone (Figure 1). They form a succession of three E-W trending, parallel fold structures, the Mail Arrouy, Sarrance, and Layens anticlines, bounded by north and south verging, post-Cenomanian thrusts (Casteras et al., 1970; Figure 2). The prerift stratigraphic sequence of the Chaînons Béarnais includes basal Keuper evaporites, breccia, and ophites and is followed by Mesozoic

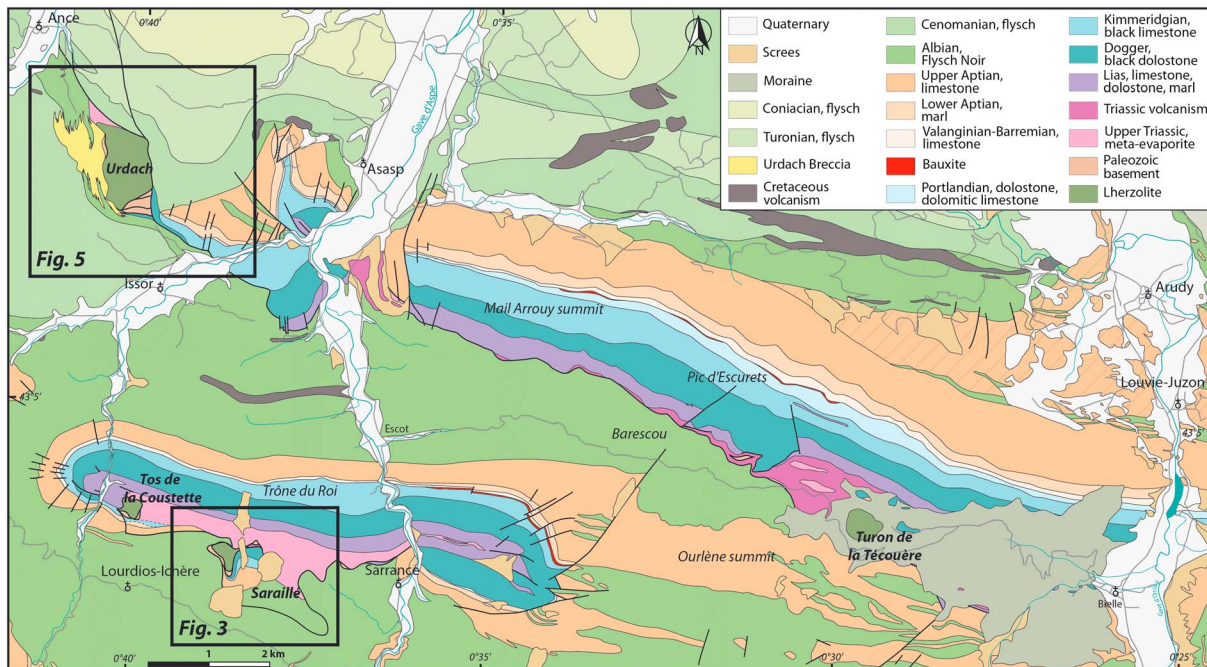


Figure 2. Geological map of the Chaînons Béarnais.

platform carbonates, both forming the original cover of the northern Iberian margin (Canérot et al., 1978; Canérot & Delavaux, 1986). The platform carbonates include Lower Jurassic dolomites and Upper Jurassic to Aptian platform limestones and form the present-day main relief. The Mesozoic sequence is entirely disconnected from its former Paleozoic basement, which is known only as very small tectonic slices or breccia fragments. Albian to Cenomanian flysch deposits are preserved within the synclines. Four main lherzolite bodies crop out in the Chaînons Béarnais: (1) two in the southern flank of the Sarrance anticline (Saraillé and Tos de la Coustette bodies), (2) one at the western tip of the Mail Arrouy anticline (Urdach body), and (3) one in the strongly tectonized zone of Benou, along the southern border of the Mail-Arrouy thrust structure (Turon de la Técoûère body; Figure 2).

3. Mapping and Sampling of the Saraillé and Urdach Paleozoic Units

3.1. The Saraillé Massif

3.1.1. Lithology, Structure, and Metamorphic Imprint: The Effects of the Cretaceous Extensional Event

The Saraillé massif exposes a south verging, recumbent fold which overthrusts the southern flank of the Sarrance anticline (Figure 2). The Saraillé fold involves various lithologies that compose a remarkably complete but extremely attenuated lithospheric section including mantle rocks, continental crustal rocks, and their Mesozoic sedimentary cover. Strongly thinned Mesozoic prerift carbonate sediments wrap an inner lens-shaped unit (~500-m long and ~100-m thick) made of discontinuous thin slices of sheared Paleozoic crustal rocks welded on folded serpentized lherzolites (Figure 3; Corre et al., 2016; Fortané et al., 1986; Thiébaud et al., 1992).

The Saraillé peridotites are made of 95% serpentized lherzolites and minor pyroxenites, mostly websterite (Cpx + Opx), forming numerous centimeter-thick beds within the lherzolites (Gaudichet, 1974). These pyroxenites result from refertilization processes that were well identified in other mantle bodies of the NPZ (Le Roux et al., 2007). Newly formed talc and chlorite aggregates are found in shear zones that separate the ultramafic body from the Paleozoic rocks and from the Mesozoic metasediments. In particular, the contact of the mantle rocks with the Jurassic dolostones corresponds to a metasomatic layer of strongly sheared, talc-chlorite schists, up to 15-m thick and exposed over more than 300 m, which results from intense fluid circulations coeval with mantle exhumation (Corre et al., 2018, 2016).

As described in detail in the following sections, the continental crust associated with the Saraillé mantle rocks forms thin elongated tectonic lenses of various lithologies exposed in the hinge and in the reverse flank of the recumbent fold. These lenses display a well-developed tectonic foliation parallel to the contact with the peridotites. They are dominated by highly deformed quartz-rich mylonites and chlorite- or mica-rich mylonites (Figure 4). Crustal rocks are also poorly exposed to the north of the studied area at the Laünde Pass (Casteras et al., 1970; Figure 3). Paleozoic lenses are intruded by undeformed or partly sheared, millimeter- to centimeter-thick albitite veins.

The upper Saraillé massif exposes a Mesozoic sequence including Triassic to Albian metasediments (Figure 3; Canérot & Delavaux, 1986; Casteras et al., 1970; Duée et al., 1984; Fortané et al., 1986). The badly exposed Triassic sequence is tectonically dismembered and includes a poorly organized assemblage of various calc-schists, ophites, cellular dolomites, brecciated limestones, and dolostones. The Jurassic metasediments consist of variably deformed dolomitic limestones, up to 100-m thick. The Neocomian sediments correspond to an alternation of decimetric beds of pure limestones and dolomite or phyllite-rich limestones. Dolomitization decreases toward the top of the sequence. The Upper Aptian Urganian facies platform carbonates form the top and the southern flank of the Saraillé massif (Figure 3). The Jurassic to Aptian marbles are intensively recrystallized and crosscut by numerous carbonate veins that recorded intense brines circulation expelled from the Keuper clays and evaporites during the extensional Cretaceous event (Corre et al., 2018; Salardon et al., 2017). The Albian “black flysch” is largely exposed on the southern flank of the Saraillé massif. It consists of an alternation of black marls, siltstones, and limestones, some of them strongly recrystallized and also crosscut by a network of carbonate veins.

The Saraillé carbonates are dissected by at least three generations of schistosity. In the entire Mesozoic sequence, a dominant S1 foliation always parallels the stratigraphic bedding (S0). It is generally marked at the thin-section scale by a homogeneous deformation defined by the alignment of sheared calcite crystals

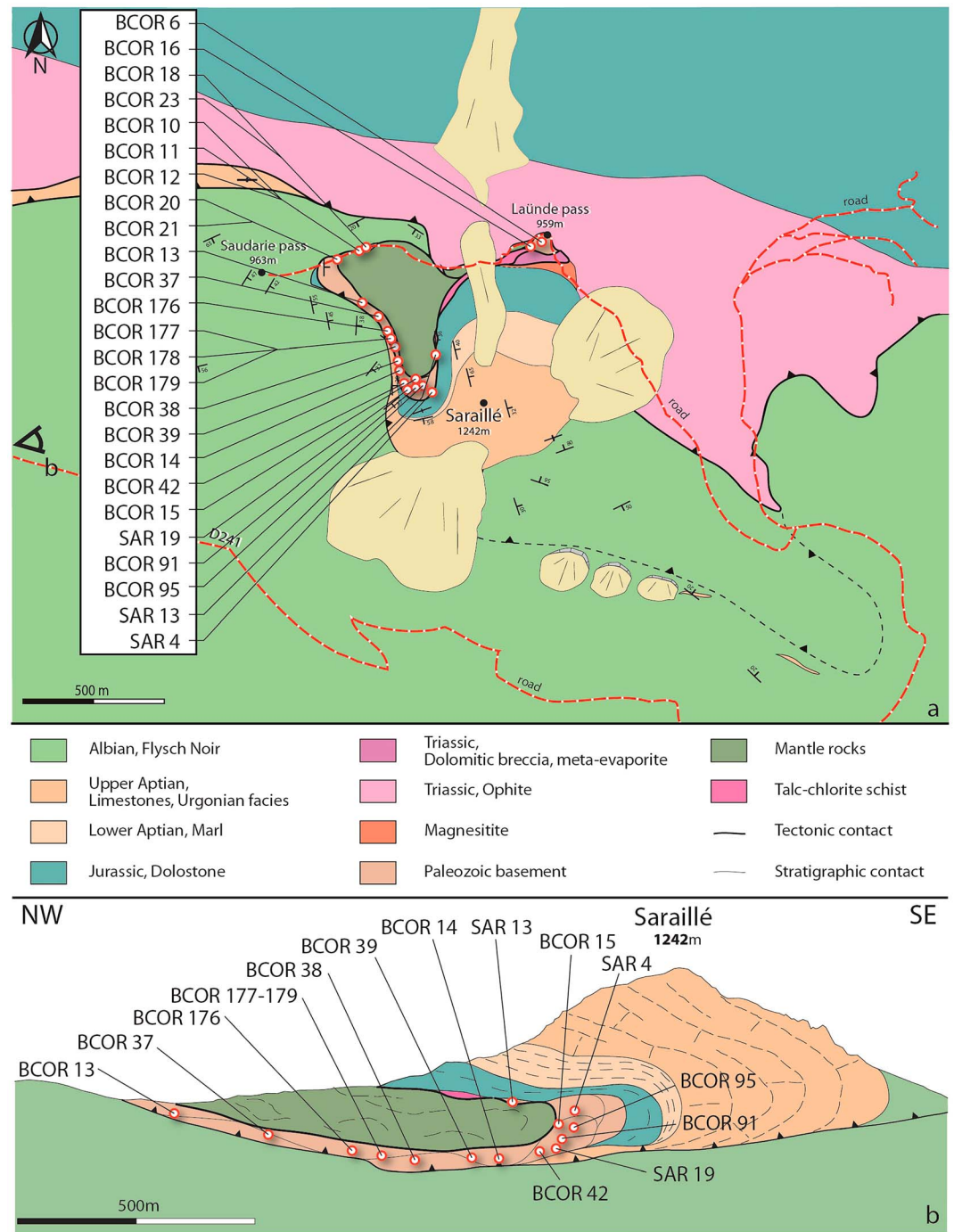


Figure 3. Geological map (a) and cross section (b) of the Saraille massif with location of the analyzed samples (redrawn and modified after Corre et al., 2018).

and by discrete shear bands paralleling S_0 in less deformed samples. The foliation is also defined by the stretching of paleontological and sedimentological objects such as macrofossils, microfossils and biogenic clasts. Numerous carbonate veins are observed at the mesoscopic and thin-section scales. The longest veins parallel the S_0 and therefore also underline the foliation. These veins are often boudinaged, indicating extension in the S_0/S_1 plane. These observations collectively indicate an early flattening of the sedimentary pile that presumably occurred during the Albian-Cenomanian extensional phase in relation with crustal thinning and subcontinental mantle exhumation (Corre et al., 2016). S_2 schistosity planes are

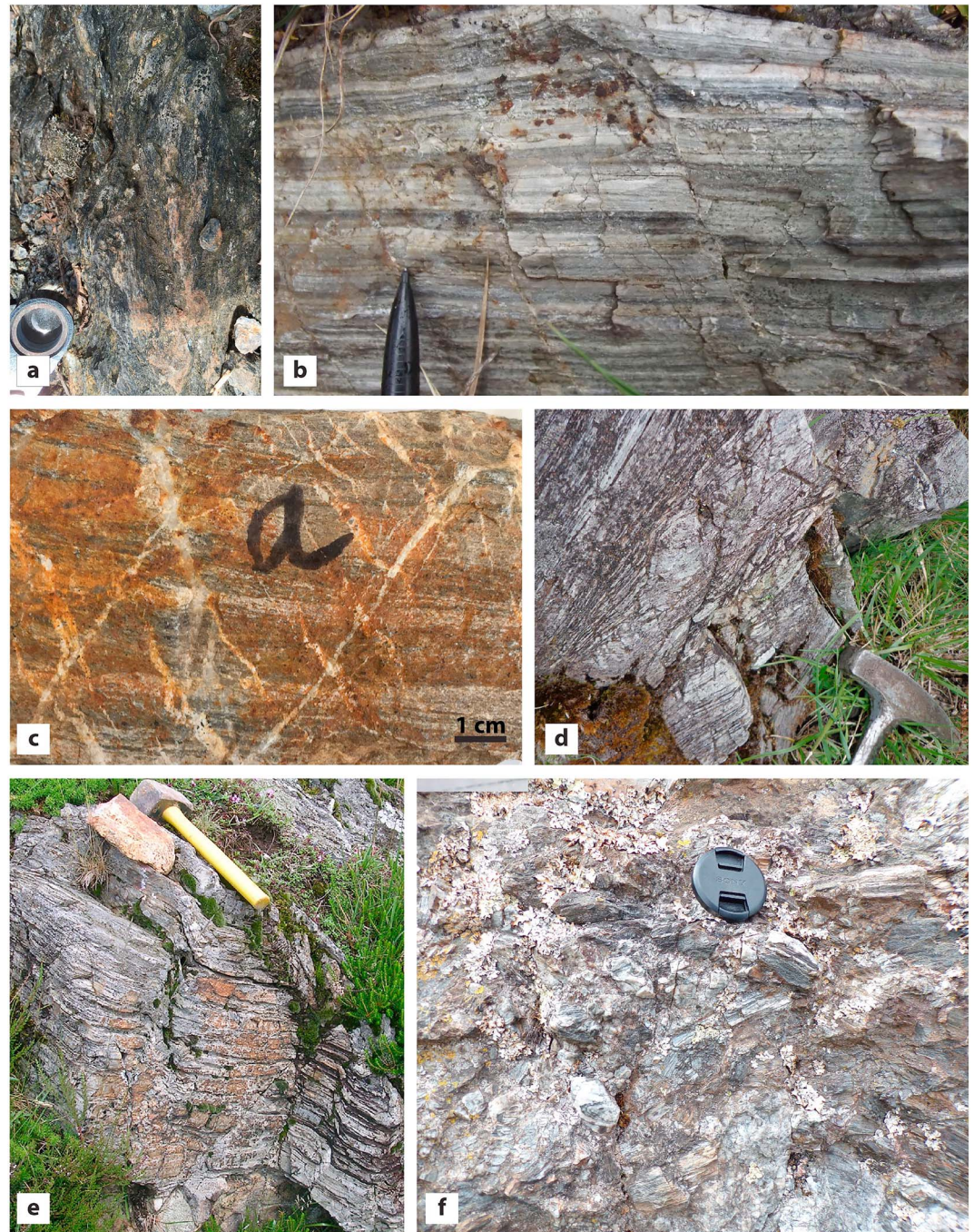


Figure 4. Outcrop pictures of crustal basement rocks exposed in the Saraillé and Urdach massifs illustrating some characteristic features of their deformation. In both massifs, the mylonitic foliation in the crustal lenses is always parallel to the contact with the mantle. (a) Example of the foliated mylonitic rocks (quartzite) outcropping in the Urdach massif. (b) Example of the deeply foliated Paleozoic metaquartzites outcropping in the Saraillé massif. (c) Network of millimetric albitite veinlets crosscutting the mylonitic foliation in a sample from the crustal basement of the Saraillé massif. (d and e) Progressive extensional brittle deformation overprinting the mylonitic fabric of crustal basement rocks at the outcrop scale. (f) Immature tectonic breccia resulting from intense brittle deformation over previously mylonitized crustal basement rocks.

subhorizontal and crosscut the S_0/S_1 foliation at low angle. These occur in the core of the recumbent fold and are parallel to its axial plane. S_3 schistosity planes are steeply dipping and roughly E-W trending. They developed in relation with the compressional stages that led to the present orogenic structure.

The thermal conditions reached by the NPZ sediments during the Cretaceous extensional event in the Saraillé area have been determined by Raman spectrometry analysis of graphitic carbon. Measurements reveal maximum temperatures of 250–350 °C in the Albian flyschs with the highest values found close to the Saraillé lherzolite (Clerc et al., 2015). This confirms previous estimates based on metamorphic assemblages of newly formed muscovite, chlorite, and albite by Gaudichet (1974), indicating greenschist facies conditions in the whole Mesozoic cover of the Sarrance anticline, including the Albian flysch. An association of talc and clinocllore, representative of greenschist facies conditions (250–350 °C), was also described by Fortané et al. (1986) in the foliated talc-rich layer representing the detachment fault separating the lherzolite from the Mesozoic sediments. Paleotemperatures recently deduced from the chemical compositions of the clinocllores from this metasomatic horizon confirm a syntectonic thermal evolution between 200 °C and 350 °C (Corre et al., 2018).

3.1.2. Sampling of the Saraillé Paleozoic Units

We collected 35 samples from the Saraillé Paleozoic basement during successive field campaigns in the following localities (Figure 3): (1) immediately south of the Laünde Pass and north of the Saraillé summit; (2) in tectonic lenses belonging to the reverse flank of the Saraillé fold and forming small exposures on the northern flank of the massif, between the Laünde Pass and the Saudarie Pass; (3) in tectonic lenses exposed in the southwest flank of the massif also belonging to the reverse limb of the Saraillé fold; they form the largest outcrops of continental basement in the study area and offer a wide variety of lithologies; and (4) in very thin lenses that belong to the normal limb of the Saraillé fold, close to the talc-chlorite layer, in an area where the continental units drastically thin and completely disappear northward.

3.2. The Urdach Massif

3.2.1. Field Evidence for Cretaceous Mantle Denudation and for the Behavior of the Paleozoic Rocks

The Urdach body is a 1.5-km long exposure of serpentinized lherzolite located in the western termination of the Mail Arrouy thrust sheet, at the boundary with the Albian and the Cenomanian flysch, between the Urdach Pass and the Etche Pass (Figure 5). The Urdach massif is well known for the occurrence of spectacular sedimentary breccia (Casteras et al., 1970), named the Urdach Breccia hereafter, composed of meter-sized clasts of talcified and serpentinized mantle rocks mixed with fragments of sheared Paleozoic basement rocks and minor Mesozoic metasediments. As agreed by all authors, the sedimentary reworking of such polymictic material indicates that a composite basement of mantle lherzolites and juxtaposed slices of continental crust has been exposed on the seafloor of the future NPZ basins during the Upper Cretaceous (Debroas et al., 2010; Fortané et al., 1986; Jammes et al., 2009; Lagabrielle et al., 2010). Moreover, the occurrence of ophicarbonates breccia and the presence of limestones infilling fissures within the Urdach ultramafics, as observed in a quarry on the western side the lherzolite body (Bilatré quarry), confirms that the mantle rocks were exposed (at least locally) on the seafloor of the former NPZ basins (Clerc et al., 2014; DeFelipe et al., 2017; Jammes et al., 2009). Dip measurements reveal that the Urdach Breccia and the Albian-Cenomanian flysch layers are involved in a kilometer-scale overturned fold with the ultramafic basement in its core.

Up to now, three major interpretations were proposed to account for the geological features of the Urdach area. They involve the following processes: (1) emplacement of large-scale composite olistolith of mantle-crustal basement in the Albian-Cenomanian flyschs along with coarse sedimentary breccia (Duée et al., 1984; Fortané et al., 1986); (2) mantle denudation along the Urdach transverse (N-S) fault scarp zone responsible for the formation of the Mid-Cretaceous Urdach composite breccia wedge (Canérot, 2017; Debroas et al., 2010); and (3) thrusting of a slice of mantle rocks and its cover of tectonosedimentary breccia over verticalized Cretaceous flysch strata (Jammes et al., 2009; Lagabrielle et al., 2010).

In agreement with Debroas et al. (2010), we confirm that the western part of the Urdach body (Soum d'Ombret) consists of a sedimentary breccia, composed of a variety of rocks including clasts of serpentinized ultramafic rocks (often talcified), numerous crustal mylonites, minor granite, gneisses, and mica schists, and rare mafic rocks (Figure 6). A chaotic assemblage of large blocks of continental material and sheared serpentinites is well exposed along the road cut, south of Soum d'Ombret. An unsorted breccia, with

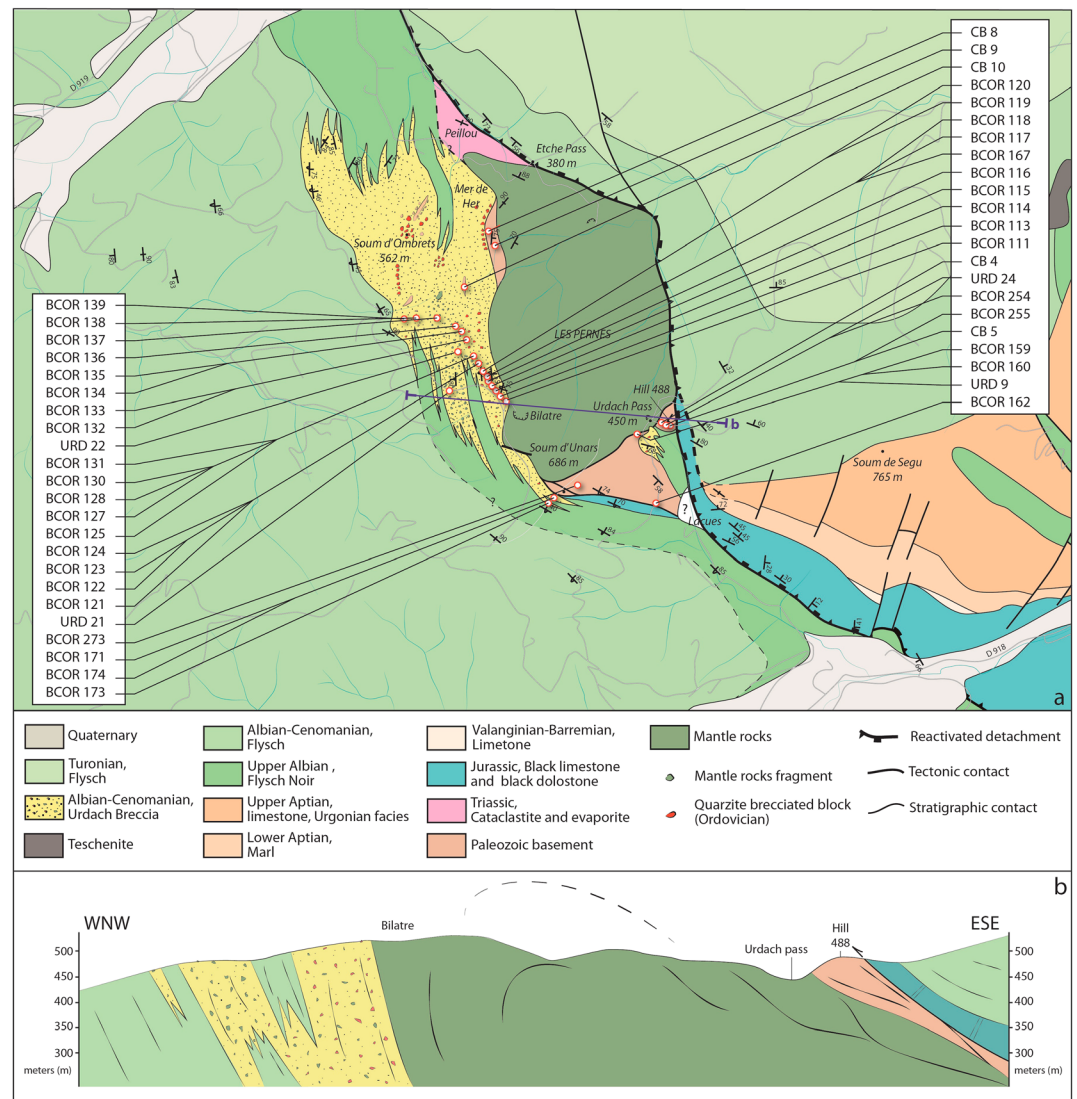


Figure 5. Geological map (a) and cross section (b) of the Urdach massif with location of the analyzed samples.

angular basement clasts including crustal mylonites, forms meter-thick layers interbedded within graded sandstones and pelites representing the dominant material of the Albian-Cenomanian flysch.

In various places, the mantle rocks are closely associated with hectometric lenses of intensively sheared Paleozoic rocks, only a few meters thick, that appear immediately beneath the Urdach Breccia. The foliation of these crustal lenses is always parallel to the geological boundary of the mantle rocks. Some of these lenses have been reported on the geological 1/50.000 Oloron-Ste-Marie geological sheet (Casteras et al., 1970), despite their location was not well constrained. The main lenses can be listed as follows (some of them will be better described in section 4). (1) South of the Etche Pass, at Mer de Her, a 500-m long unit of Paleozoic mica schists is reported as S3–2 Silurian rocks on the Oloron-Ste-Marie sheet. (2) At Soum dUnars, the peridotites are in vertical contact with a unit of strongly sheared Silurian massive black schists also reported as S3–2 Silurian rocks on the Oloron-Ste-Marie sheet. The occurrence of different crustal lithologies reworked as loose blocks in the slopes around Soum dUnars may suggest that the lens of sheared Silurian black schists is capped by relicts of the Urdach Breccia. (3) Along the road to the Urdach Pass the occurrence of a layer of sheared andalusite-bearing mica schist is deduced from the presence of numerous debris derived from this protolith. The poor outcrop conditions preclude to map the exact shape of this small lens. Exposures along the road cut at Grange Lacues (SE of the Urdach massif) show various crustal lithologies, dominantly



Figure 6. Outcrop pictures of the Urdach Breccia. (a and e) Characteristic aspect of the Urdach Breccia; black arrows indicate centimetric to decimetric clasts of talcified mantle rocks reworked together with crustal lithologies in the breccia. (b and d) Clasts of intensely foliated mylonitic crustal rocks (quartzite) reworked in the breccia. (c) Clast of foliated mylonitic crustal rock (quartzite) overprinted by a progressive brittle deformation (as in Figures 4d and 4e) reworked in the breccia. (f) Example of the quartz-cemented tectonic breccia; this breccia can be found reworked as clasts in the Urdach Breccia.

mylonitized, within a reddish argillaceous matrix and confirm that the Urdach Breccia is exposed along the southern border of the Urdach mantle body up to the Urdach Pass. (4) Some meters east of the Urdach Pass, a small hill, referred to as “hill 488” hereafter, consists of variously sheared mica schists and porphyric leptynites. This outcrop has been previously mapped as a granite on the 1/50.000 Oloron-Ste-Marie geological sheet.

3.2.2. Sampling of the Urdach Paleozoic Units

We collected 56 samples from the Urdach Paleozoic basement during successive field campaigns in different formations (Figure 5). (1) Massive rocks were sampled at three localities: (i) immediately east of the Urdach Pass on the southern flank of hill 488, (ii) at Soum dUnars, and (iii) on the eastern flank of Soum dOmbrets at Mer de Her. (2) Samples from various types of clasts in the Urdach Breccia were collected at different localities, (i) south of Soum dOmbrets and (ii) at Bilatre.

4. Lithology and Deformation of the Continental Basement Units

4.1. Lithology of Crustal Rocks in Contact with the Exhumed Mantle

As presented above, geological mapping shows that various types of Variscan rocks are currently lying in direct contact with the mantle rocks. In the Saraillé massif, we observe the following lithologies in contact with the lherzolites: (i) to the north, mylonitic andalusite-mica schists (Launde), gneisses with abundant albitite veins (Saudarie); and (ii) on the southwestern flank, thinly banded quartzitic ultramylonite, impure marbles, mica schists, variably mylonitized orthogneisses and chloritized paragneisses. In the Urdach massif, massive crustal units in contact with the lherzolites are (from east to west) (i) mylonitic leptynites and paragneisses at hill 488, (ii) dominant andalusite schists and Silurian black schists at Soum dUnars, and (iii) Silurian black schists and Ordovician quartzites at Mer de Her. In Urdach, mapping information reveals rapid lithologic variations of the crustal rocks, suggesting a geological structure of small lenticular units. These small units relate mostly to granitoids and amphibolite to greenschist facies metamorphic rocks, well known in the Variscan basement of the Pyrenees.

4.2. Lithology of Clasts in the Urdach Breccia

The Urdach Breccia provides a unique opportunity to sample a wide variety of crustal lithologies exhumed during the Cretaceous rifting. Beside fragments of serpentinized and talcified lherzolites, the breccia contains angular clasts of undeformed to cataclastic granitoids, gneissic granitoids, various types of mica schists (some of them bearing andalusite or garnet porphyroblasts), abundant thinly layered quartz-rich mylonites (previously considered as thinly bedded quartzites by Fortané et al., 1986), thinly foliated black schists, chlorite schists, and rare Jurassic and Cretaceous marbles (Figure 6). Albitite clasts derived from corundum- and zircon-bearing magmatic albitite intrusions crosscutting the ultramafic massif (Monchoux et al., 2006; Pin et al., 2001; Pin et al., 2006) are also found reworked in the breccia. Close to Mer de Her, to the NW of the massif, the breccia is monogenic and bears the characteristics of a tectonic breccia (Figures 4f and 6f). It consists of an accumulation of angular clasts of likely Ordovician quartzites and is devoid of sedimentary features. Large volumes of this breccia are strongly cemented by quartz, often geodic, locally coated by iron oxides. The tectonic brecciation and the quartz cementation likely occurred before exposure of the breccia to the seafloor, when the cataclastic rocks were still forming a coherent tectonic unit within the exhumation fault system.

It is worth noting that no Paleozoic rock younger than Silurian has been found among the clasts composing the Urdach Breccia, nor in the crustal lenses enveloping the ultramafic Urdach and Saraillé massifs.

4.3. Deformation and Microstructures of Crustal Rocks: The Saraillé and Urdach Basement Units and a Selection of Clasts from the Urdach Breccia

A summary of the observations in thin sections from crustal samples in the Saraillé and in the Urdach massifs, including information on the mineral assemblage as well as the intensity of the deformation, is presented in Table 1.

Crustal lithologies exposed along the contact with the mantle rocks or reworked as pebbles in the Urdach Breccia vary from para-derived mylonitic rocks to ortho-derived rocks (see sections 4.1 and 4.2) showing variable degrees of deformation. It is worth to note that many samples show evidence for late-mylonitic to postmylonitic quartz and albite veining crosscutting the mylonitic foliation. Moreover, much evidence exists for a late-mylonitic to postmylonitic event of hydrothermal fluids circulation, which led to a more or less pronounced chloritization and/or albitization of the crustal rocks; the intensity of this metasomatic event sometimes resulted in a complete obliteration of the previous metamorphic textures (e.g., BCOR 115).

In the Saraillé massif, para-derived metamorphic rocks are mostly represented by mylonitic chiasmolite-bearing black mica schists; shear foliation is defined by white mica and microcrystalline quartz and wraps around andalusite porphyroblasts, which typically show symmetric ϕ -type geometry (e.g., Figure 7a) and occasionally σ -type geometry with contrasting senses of shear. Quartzitic layers on the western flank of the massif show various degrees of deformation, ranging from almost undeformed (e.g., BCOR 37a) to S-L tectonites (e.g., BCOR 13) with quartz dynamically recrystallized to form polycrystalline ribbons (e.g., Figures 8b and 8c). Minor impure marbles (amphibole-quartz-plagioclase-bearing) are also present in the

Table 1
Lithology, Mineralogical Composition and Characterization of the Deformation in the Crustal Rocks Analyzed in the Sarailié and the Urdach Massifs (From Outcropping Crustal Lenses or Reworked as Clasts in the Urdach Breccia)

Sample name	Massif	Breccia/bedrock	Rock type	Mineral composition	Type of deformation	Quartz recrystallization microstructures	T max of deformation	Deformation intensity
SAR4a	Sarailié	Bedrock	Black mica schist with Ab veins	Ms, Ab, Qz (?), Gr	M (with cataclastic overprint)		?	++
SAR13	Sarailié	Bedrock	Chlorito-schist	Chl, Py	M/UM (?)		?	++/++++ (?)
SAR16	Sarailié	Bedrock	Chlorito (talc)-schist with Ab veins	Chl, Tlc, Ab, Qz, Py (+ Ap?)	UM (with cataclastic overprint)		?	+++
SAR18	Sarailié	Bedrock	Granitoid	Qz, Kfs, Pl (+ Ms)	PM (not foliated)	UE, BLG, NCL, SGR	400–500 °C	+
SAR19a	Sarailié	Bedrock	Granitoid	Qz, Pl, Kfs, Chl	PM (not foliated)	UE, BLG, NCL, SGR	400–500 °C	+
SAR19b	Sarailié	Bedrock	Mylonitic orthogneiss	Qz, Kfs, Ms, Chl (+ Pl in veins)	UM	PCR, BLG, NCL, SGR	400–500 °C	++/++++
SAR19c	Sarailié	Bedrock	Orthogneiss	Pl, Chl, Qz, Amp, Bt, Kfs, Ms	Mylonite with cataclastic overprint	PCR, BLG, NCL, SGR	400–500 °C	++
SAR23	Sarailié	Bedrock	Mylonitic orthogneiss with Ab veins	Qz, Kfs (Ser), Ab	Mylonite	MCR, PCR, BLG, NCL, SGR	400–500 °C	++
BCOR6a	Sarailié	Bedrock	Chiaistolie-bearing black schist	Qz, Ms, Gr, And	M		(?)	++
BCOR6b	Sarailié	Bedrock	Chiaistolie-bearing black schist	Qz, Ms, Gr, And	M			++
BCOR6c	Sarailié	Bedrock	Chiaistolie-bearing black schist	Qz, Ms, Gr, And, Pl (in veins)	M			++
BCOR6d	Sarailié	Bedrock	Chiaistolie-bearing black schist	Qz, Ms, Gr, And	M			++
BCOR10	Sarailié	Bedrock	Chloritized (ortho?)gneiss	Qz, Chl, Fsp (+Py?)	M	?	?	++
BCOR11	Sarailié	Bedrock	Granitoid	Qz, Kfs, Pl, Chl (+Py)	PM (not foliated)	UE, BLG, NCL, SGR	400–500 °C	+
BCOR12a	Sarailié	Bedrock	Phyllonite with Qz veins	Qz, Ms, Chl (+Py)	UM	BLG, NCL, SGR	400–500 °C	+++
BCOR12b	Sarailié	Bedrock	Orthogneiss with Ab veins	Qz, Kfs, Ms (?), Chl (?), Ab (+Py)	M	PCR	?	++
BCOR13	Sarailié	Bedrock	Quartzitic Ultramylonite	Qz, Ms, Chl (?) (+Py)	UM	PCR	?	+++
BCOR14	Sarailié	Bedrock	Contact between (ortho?)gneiss and graphitic-bearing mica schist	Pl, Kfs (?), Qz, Chl, Bt, Ms (?), Qz, Ms, Gr, Chl	M	BLG, SGR	400–500 °C	++
BCOR15	Sarailié	Bedrock	Cataclastic melange of orthogneiss and ultramylonite	Qz, Pl, Ms, Kfs (Ser) (+Tur)	M + UM	MCR, PCR, BLG, SGR	400–500 °C	++/++++
BCOR20	Sarailié	Bedrock	Orthogneiss with Ab veins	Pl, Kfs, Qz, Chl, Ms (+Py)	M	UE, MCR, PCR, BLG, NCL, SGR	400–500 °C	++
BCOR21	Sarailié	Bedrock	Chloritized ultramylonite with chlor veins	Chl, Qz, Pl, Ms (+Py)	UM	BLG, NCL, SGR	400–500 °C	+++
BCOR37a	Sarailié	Bedrock	Quartzite	Qz, Ms	Almost UND	UE	>300 °C	–
BCOR37b	Sarailié	Bedrock	Chloritized felsic gneiss	Chl, Fsp (Ser), Qz	(?)	?	?	– (?)
BCOR37c	Sarailié	Bedrock	Chloritized felsic gneiss	Chl, Fsp (Ser), Qz	(?)	?	?	– (?)
BCOR38a	Sarailié	Bedrock	Phyllonite	Qz, Ms (+Py)	UM	UE, BLG, SGR	400–500 °C	+++
BCOR38b	Sarailié	Bedrock	Phyllonite	Qz, Ms (+Py)	UM	UE, BLG, SGR	400–500 °C	+++
BCOR38c	Sarailié	Bedrock	Granitoid	Qz, Kfs, Pl, Ms (+Py)	PM (not foliated)	UE, BLG, NCL, SGR	400–500 °C	+
BCOR39	Sarailié	Bedrock	(Amphibolitic?) Gneiss	Qz, Amp (Hbl), Ep, Pl (?)	M	BLG, SGR	400–500 °C	++
BCOR42	Sarailié	Bedrock	Phyllonite	Qz, Ms, Chl	UM	(?)	(?)	+++
BCOR91	Sarailié	Bedrock	Amphibolitic (?) Marble	Cb, Amp (Hbl), Qz, Pl (+Ttn)	M (?)			++ (?)
BCOR95	Sarailié	Bedrock	And-bearing black schist	Gr, Qz, And, Chl, Ms (?)	M	?	?	++
BCOR176	Sarailié	Bedrock	Granitoid	Kfs, Pl, Qz, Chl, Bt, Ms	PM (not foliated)	MCR, PCR, UE, SGR	400–500 °C	+

Table 1 (continued)

Sample name	Massif	Breccia/bedrock	Rock type	Mineral composition	Type of deformation	Quartz recrystallization microstructures	T max of deformation °C	Deformation intensity
BCOR177	Sarailé	Bedrock	Orthogneiss	Qz, Kfs, Ms, Chl, Grt	M/UM	SGR (?)	400–500 °C (?)	++/++++
BCOR178	Sarailé	Bedrock	Orthogneiss	Kfs, Pl, Qz, Chl, Bt, Ms	M	MCR, PCR, BLG, SGR	400–500 °C	++
BCOR179	Sarailé	Bedrock	Granitoid	Pl, Qz, Kfs, Chl, Bt, Ms	PM (not foliated)	UE, BLG, SGR	400–500 °C	+
URD9-1	Urdach	Bedrock	Abitite (abitized granitoid?)	Pl, Kfs (Ser), Chl, Ms (+ Zrn)	UND	–	–	–
URD9-2	Urdach	Bedrock	Chloritized Qz-pegmatite	Chl, Qz, Pl (?) (+Fe oxides)	UND	–	–	–
URD21a	Urdach	Breccia clast	Garnet mica schist	Qz, Ms, Bt, Grt, Chl (?), Tic (?)	M	MCR, PCR, SGR	400–500 °C	++
URD21b	Urdach	Breccia clast	Mica schist	Ms, Qz, Bt, Fsp (?) (+Fe oxides)	M	PCR, SGR(?)	?	++
URD21d	Urdach	Breccia clast	Mica schist	Ms, Qz (+ rounded Zrn)	M	PCR, SGR(?)	?	++
URD22a	Urdach	Breccia clast	Quartzite	Qz, Ms (+Rt, Zrn)	M	MCR, PCR, SGR	400–500 °C	++
URD22b	Urdach	Breccia clast	Qz-pegmatite	Qz	PM	UE, BLG, NCL, little SGR(?)	<400 °C (?)	+
URD22c	Urdach	Breccia clast	Chiaistolite-bearing mica schist	Qz, Ms, And, Bt, Chl	UND to PM	–	–	-/(?)
URD22d	Urdach	Breccia clast	Chiaistolite-bearing mica schist	Ms, Qz, Chl, And	M	?	?	++
URD24a	Urdach	Bedrock	Mica schist/quartzite	Qz, Ms (?), Pl, Kfs	UM	BLG, NCL	300–400 °C	+++
URD24b	Urdach	Bedrock	(Leucocratic) Orthogneiss	Qz, Ms, Kfs, Pl	M	PCR, BLG	300–400 °C	++
BCOR111	Urdach	Breccia clast	Ultramylonite	Ms, Qz, Chl, Pl (in veins) (+Tur)	UM	?	?	+++
BCOR113	Urdach	Breccia clast	Ultramylonite	Qz, Ms	UM	PCR, BLG, SGR (?)	400–500 °C (?)	+++
BCOR114	Urdach	Breccia clast	Partially abitized granitoid	Qz, Pl, Kfs, Ms, Bt, Chl (+ Zrn)	UND	–	–	–
BCOR115	Urdach	Breccia clast	Chloritite	Chl, Zrn	UND (?)	–	–	– (?)
BCOR116	Urdach	Breccia clast	Quartzite	Qz, Ms, Bt, Tur	M/UM	MCR, PCR, BLG, SGR	400–500 °C	++/++++
BCOR117	Urdach	Breccia clast	Chiaistolite-bearing mica schist	Chl, Ms, Qz, And, Bt	M	?	?	++
BCOR118	Urdach	Breccia clast	Quartzite	Qz, Tur	UM	MCR, PCR, BLG, SGR (?)	400–500 °C (?)	+++
BCOR119	Urdach	Breccia clast	Granitoid	Pl, Qz, Bt, Kfs	PM (not foliated)	UE, BLG, NCL, little SGR(?)	~400 °C (?)	+
BCOR120	Urdach	Breccia clast	Granitoid	Pl, Bt, Qz, Kfs	PM (not foliated)	UE, BLG, NCL, little SGR(?)	~400 °C (?)	+
BCOR121	Urdach	Breccia clast	Granitoid	Pl, Qz, Bt, Kfs	PM (not foliated)	UE, BLG, NCL, little SGR(?)	~400 °C (?)	+
BCOR122	Urdach	Breccia clast	Quartzite	Qz, Ms, Chl (+ rounded Zrn)	M/UM	UE, PCR, BLG, SGR (?)	400–500 °C (?)	++/++++
BCOR123a	Urdach	Breccia clast	(Amphibolitic?) Gneiss	Qz, Amp (Hbl), Ep, Pl, Grt	M	UE, MCR, PCR, BLG, SGR (?)	400–500 °C	++
BCOR123b	Urdach	Breccia clast	Quartzite	Qz, Ms, Bt, Tur (?) (+ rounded Zrn)	M	UE, PCR, BLG, SGR (?)	400–500 °C (?)	++

Table 1 (continued)

Sample name	Massif	Breccia/bedrock	Rock type	Mineral composition	Type of deformation	Quartz recrystallization microstructures	T max of deformation	Deformation intensity
BCOR124	Urdach	Breccia clast	Mica schist	Bt, Ms, Qz, Sil	M	UE, BLG, SGR (?)	400–500 °C (?)	++
BCOR125	Urdach	Breccia clast	Qz/Tur-pegmatite	Qz, Tur	PM (not foliated)	UE, NCL, BLG, little SGR (?)	400–500 °C (?)	+
BCOR127	Urdach	Breccia clast	Mica schist	Ms, Qz, Chl	M	(In Ms: MF)	~400 °C (?)	++
BCOR128	Urdach	Breccia clast	Qz-Diorite	Pl, Bt (+ Qz)	UND	UE	–	–
BCOR130	Urdach	Breccia clast	Bt-bearing Quartzite	Qz, Bt, Ms, Chl	M/UM	MCR, PCR, BLG, SGR	400–500 °C	++/+++
BCOR131	Urdach	Breccia clast	Granitoid	Pl, Bt, Qz	PM (not foliated)	UE, BLG, NCL, little SGR (?)	~400 °C (?)	+
BCOR132	Urdach	Breccia clast	Quartzite	Qz, Ms, Chl, Tur (+ rounded Zrn)	M	UE, PCR, BLG, SGR (?)	400–500 °C (?)	++
BCOR133	Urdach	Breccia clast	Quartzite + mica schist	Qz, Ms (+ Gr, rounded Zrn)	M	MCR, PCR, BLG, SGR (?)	400–500 °C (?)	++
BCOR134	Urdach	Breccia clast	Quartzite + mica schist	Qz, Ms	M	In Ms: MF	400–500 °C (?)	++
BCOR135	Urdach	Breccia clast	Quartzite	Qz (+ rounded Zrn)	M/UM	UE, PCR, BLG, SGR	400–500 °C (?)	++/+++
BCOR136	Urdach	Breccia clast	Ultramylonite with cataclastic overprint	Qz, Ms	UM	?	?	+++
BCOR137	Urdach	Breccia clast	Quartzitic mica schist (?)	Qz, Ms, Bt (?) (+ Tur)	M	UE, PCR, NCL, BLG, SGR	400–500 °C	++
BCOR138	Urdach	Breccia clast	Granitoid	Pl, Qz, Kfs, Bt, Ms	PM (not foliated)	UE, BLG, NCL, SGR	400–500 °C	+
BCOR139	Urdach	Breccia clast	Mica schist/paragneiss	Ms, Bt, Qz (+ Rt)	M	NCL, BLG, SGR (?)	40–500 °C (?)	++
BCOR159	Urdach	Breccia clast	Quartzite	Qz, Ms, Chl (in veins)	M/UM	UE, NCL, BLG, GBM	500–600 °C	++/+++
BCOR160	Urdach	Breccia clast	Qz-pegmatite	Qz, Chl	UND	–	–	–
BCOR162	Urdach	Bedrock	Mica schist	Ms/Tlc (?), Bt, Chl, Qz	M/UM	BLG, SGR (?)	400–500 °C (?)	++/+++
BCOR167	Urdach	Breccia clast	Mica schist	Qz, Ms, Bt (+ Tur)	M	UE, NCL, BLG, SGR	400–500 °C	++
BCOR171	Urdach	Breccia clast	Black mica schist	Ms, Bt, Graph, Qz	M/UM (?)	?	?	++/+++ (?)
BCOR173	Urdach	Breccia clast	Granitoid (leucocratic)	Pl, Qz, Kfs, Chl (in veins)	PM (not foliated)	UE, BLG, NCL	300–400 °C	+
BCOR174	Urdach	Breccia clast	(Leucocratic) Orthogneiss	Qz, Kfs, Ms, Pl (+ Grt)	M	PCR, BLG	300–400 °C	++
BCOR254a	Urdach	Bedrock	Mica schist/quartzite	Qz, Ms, Chl, Kfs, Grt, Pl	UM	NCL (?), BLG (?)	300–400 °C (?)	+++
BCOR254b	Urdach	Bedrock	(Leucocratic) Orthogneiss	Qz, Kfs, Ms, Pl	M	UE, BLG, NCL	300–400 °C	++
BCOR254c	Urdach	Bedrock	Mica schist/quartzite	Qz, Ms, Chl, Kfs, Grt, Pl	UM	NCL (?), BLG (?)	300–400 °C (?)	+++
BCOR255	Urdach	Bedrock	(Leucocratic) orthogneiss	Qz, Kfs, Ms, Pl	M	UE, BLG, NCL	300–400 °C	++

Table 1 (continued)

Sample name	Massif	Breccia/bedrock	Rock type	Mineral composition	Type of deformation	Quartz recrystallization microstructures	T max of deformation	Deformation intensity
BCOR273	Urdach	Breccia clast	Qz-pegmatite	Qz (+ Chl in fractures)	PM (not foliated)	UE, BLG, NCL	300–400 °C	+
CB4	Urdach	Bedrock	(Leucocratic) Orthogneiss	Qz, Ms (?), Kfs, Pl	M	UE, BLG, NCL	300–400 °C	++
CB5a	Urdach	Bedrock	(Ortho/para?)gneiss	Qz, Ms, Pl, Kfs	M	UE, BLG	300–400 °C	++
CB5c	Urdach	Bedrock	(Ortho/para?)gneiss	Qz, Ms, Pl, Kfs	M	UE, BLG	300–400 °C	++
CB8	Urdach	Bedrock	Quartzite	Qz, Ms, Chl (?) (+Fe oxides)	M	UE, BLG (?)	300–400 °C (?)	++
CB9	Urdach	Bedrock	Quartzite	Qz, Chl, Ms (+Zrn)	PM	UE, BLG (?)	300–400 °C (?)	+(?)
CB10	Urdach	Breccia Clast	(Leucocratic) Orthogneiss	Qz, Ms, Kfs, Pl	M	PCR, BLG, SGR	400–500 °C	++

Note. Abbreviations for mineral names are after Whitney and Evans (2010). Abbreviations for type of deformation: UND = undeformed; PM = protomylonite; M = mylonite; UM = ultramylonite. Abbreviations for quartz recrystallization microstructures: UE = undulose extinction; MCR = monocrySTALLINE ribbons; PCR = polycrySTALLINE ribbons; BLG = bulging; NCL = nucleation; SGR = subgrain rotation; GBM = grain boundary migration; MF = mica fish.

southern part of the massif, showing high degrees of deformation of the microcrystalline carbonate matrix resulting in sheath folds and recumbent microfolds at the scale of the thin section.

Ortho-derived rocks in the Sarailé massif show a variety of degrees of deformation (Figures 7c–7e), ranging from weakly deformed cataclastic/protomylonitic granodioritic rocks to phyllonitic ultramylonites. In the weakly deformed granitoid rocks, even though deformation was not intense enough to produce a well-developed tectonic foliation, quartz always shows some evidence for dynamic recrystallization (Figure 7d). In mylonitic to ultramylonitic orthogneisses, a quartz + biotite ± muscovite tectonic foliation progressively overprinted the previous magmatic texture (Figure 7e). The shear foliation wraps around more or less sericitized feldspar porphyroclasts to produce augen, generally showing a ϕ -type and occasionally a σ -type geometry with contrasting senses of shear (Figure 7e). Feldspar response to deformation is generally brittle, with evidence for microfracturing, undulose extinction, and bent twins; evidence for dynamic recrystallization of feldspar is limited and, when present, it is dominantly assisted by incipient bulging at grain boundaries (e.g., Figures 7e, 8d, and 8e). Observed feldspar microstructures are compatible with maximum temperatures of deformation not exceeding 450 °C (e.g., Gapais, 1989; Passchier & Trouw, 2005; Pryer, 1993). Biotite and muscovite commonly show undulose extinction and form mica fishes (e.g., Figure 8e), thus pointing to relatively low temperatures of deformation (e.g., Passchier & Trouw, 2005). Quartz dynamic recrystallization is dominantly assisted by nucleation, bulging, and subgrain rotation and induced a more or less pronounced reduction of the grain size (increasing with the intensity of deformation) resulting in the formation of polycrystalline quartz ribbons (Figures 8a–8c). The observed quartz microstructures are compatible with maximum temperatures of deformation in the range of 400–500 °C (e.g., Drury & Urai, 1990; Hirth & Tullis, 1992; Law, 2014; Passchier & Trouw, 2005; Stipp et al., 2002). In general, in the ortho-derived rocks of the Sarailé massif, biotite has been largely altered to chlorite during deformation.

In the Urdach massif, at hill 488 the leptynitic gneiss show a mylonitic foliation defined by fine-grained, dynamically recrystallized quartz and white mica (Figures 9b and 9c). Feldspar exhibits brittle behavior and locally shows evidence for cataclastic flow at grain boundaries; the tectonic foliation wraps around feldspar porphyroclasts to form augen, which typically show σ -type geometry with a top-to-the-ENE sense of shear (Figures 9a–9c). Large-size muscovites show undulose extinction and form mica fishes pointing to a top-to-the-ENE sense of shear coherent with that displayed by the feldspar σ types (Figures 9b and 9c), thus pointing to relatively low temperatures of deformation (e.g., Passchier & Trouw, 2005). Dynamic recrystallization of quartz is dominantly assisted by nucleation and bulging, with scarce evidence for subgrain rotation recrystallization, and led to grain size reduction (Figure 8). The observed microstructures are compatible with maximum temperatures of deformation in the order of ~400 °C (e.g., Drury & Urai, 1990; Hirth & Tullis, 1992; Law, 2014; Passchier & Trouw, 2005; Stipp et al., 2002). The leptynitic gneisses are interfingered with highly deformed fine-grained chloritized quartzitic mica schists, bearing feldspar and garnet porphyroclasts and displaying isoclinal microfolds at the scale of the thin section (Figure 7h).

In the Urdach Breccia, most of the para-derived samples are analog to the metasedimentary Paleozoic rocks exposed in the crustal lenses to the NW and to the south of the massif, and also to the metasedimentary layers intercalated with the leptynitic gneiss at hill 488. In chistolite-bearing dark mica schists (e.g., BCOR 117) andalusite porphyroblasts are wrapped by the metamorphic foliation and produce ϕ -type geometries. In mica schist pebbles, quartz microstructures are hardly decipherable; however, grain size reduction of quartz seems to have been dominantly assisted by

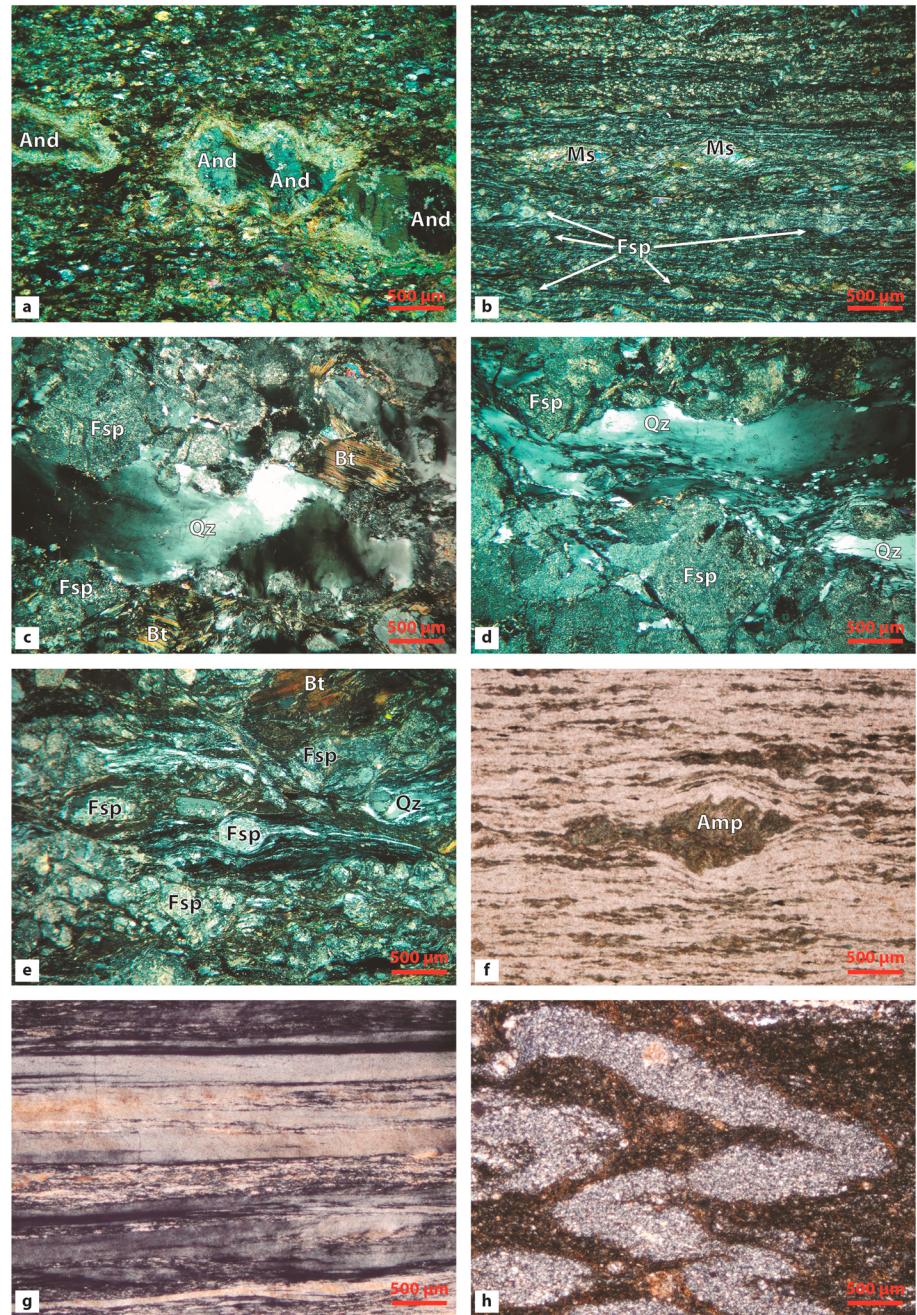


Figure 7. Thin section pictures of representative examples of crustal basement rocks from the Sarailé and Urdach massifs. (a) Mica schist with partially boudinaged φ -type andalusite porphyroclasts embedded in the foliation (crossed polarizers). (b) Mica schist with small φ -type feldspar porphyroclasts embedded in the foliation (crossed polarizers). (c) Almost undeformed granitoid sample from the Sarailé massif (crossed polarizers); the only traces of deformation are represented by undulose extinction and incipient subgrain rotation recrystallization in quartz. (d) Protomylonitic granitoid from the Sarailé massif (crossed polarizers); development of an incipient foliation is assisted by dynamic recrystallization of quartz mainly by subgrain rotation. (e) Mylonitic orthogneiss from the Sarailé massif (crossed polarizers); φ -type feldspar porphyroclasts are embedded in a strained foliation made of recrystallized quartz ribbons (deformation in quartz is dominantly assisted by subgrain rotation recrystallization). (f) Gneiss with φ -type amphibole porphyroclasts embedded in the foliation from the Urdach Breccia (plane polarized light). (g) Ultramylonitic quartzite from the Urdach Breccia with alternating monocrystalline and polycrystalline quartz ribbons (crossed polarizers). (h) Isoclinal microfolds in a quartzite/mica schist sample from the crustal basement of the Urdach massif (crossed polarizers).

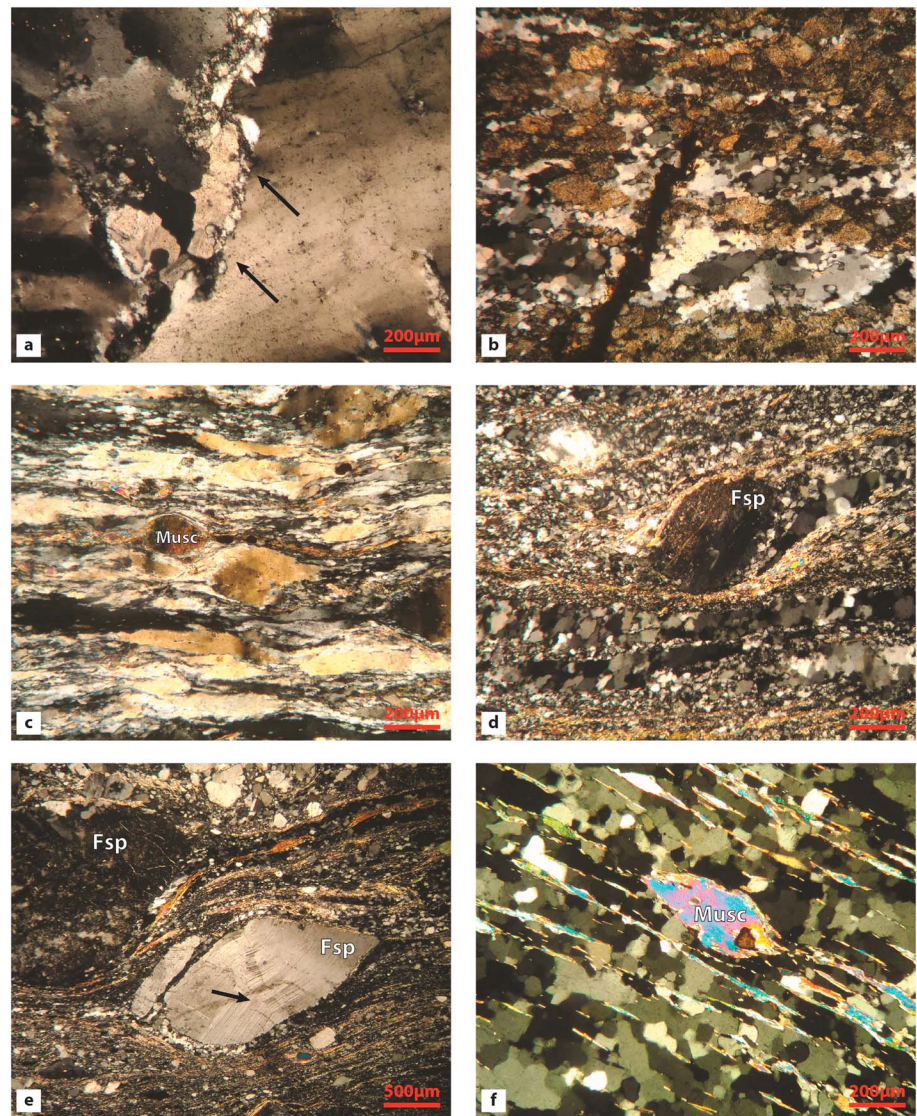


Figure 8. Examples of recrystallization microstructures in mylonitic crustal rocks sampled in the Urdach and Sarailé massifs. (a) Example of bulging recrystallization at crystal boundaries of quartz with undulose extinction (low temperature). (b and c) Examples of subgrain rotation recrystallization in quartz (medium temperature). (d and e) The σ -type feldspar porphyroclasts embedded in a strained foliation defined by stretched quartz and white mica with dextral sense of shear; quartz recrystallization is dominantly assisted by bulging and subgrain rotation (medium temperature). In (e), note bent twins in feldspar porphyroclast (indicated by black arrow). (f) Muscovite mica fish embedded in stretched quartz dominantly recrystallized via grain boundary migration (high temperature).

nucleation and bulging recrystallization. In the most quartzitic layers (e.g., BCOR 123b), quartz shows evidence for dynamic recrystallization also assisted by incipient subgrain rotation. The observed microstructures point to maximum temperatures of deformation in the order of ~ 400 °C (e.g., Drury & Urai, 1990; Hirth & Tullis, 1992; Law, 2014; Passchier & Trouw, 2005; Stipp et al., 2002).

The ortho-derived pebbles exposed in the Urdach Breccia show variable degrees of deformation. The most deformed mylonitic orthogneisses (e.g., BCOR 174) are akin to those sampled at hill 488. The less deformed magmatic pebbles vary from undeformed granitoids (e.g., BCOR 128) to cataclastic/protomylonitic granitoids (e.g., BCOR 131), where dynamic recrystallization of quartz was dominantly assisted by nucleation, bulging and, in some cases, subgrain rotation (e.g., BCOR 138), but shearing was not intense enough to produce a well-developed tectonic foliation; these rocks are comparable to the nonfoliated granitoid rocks

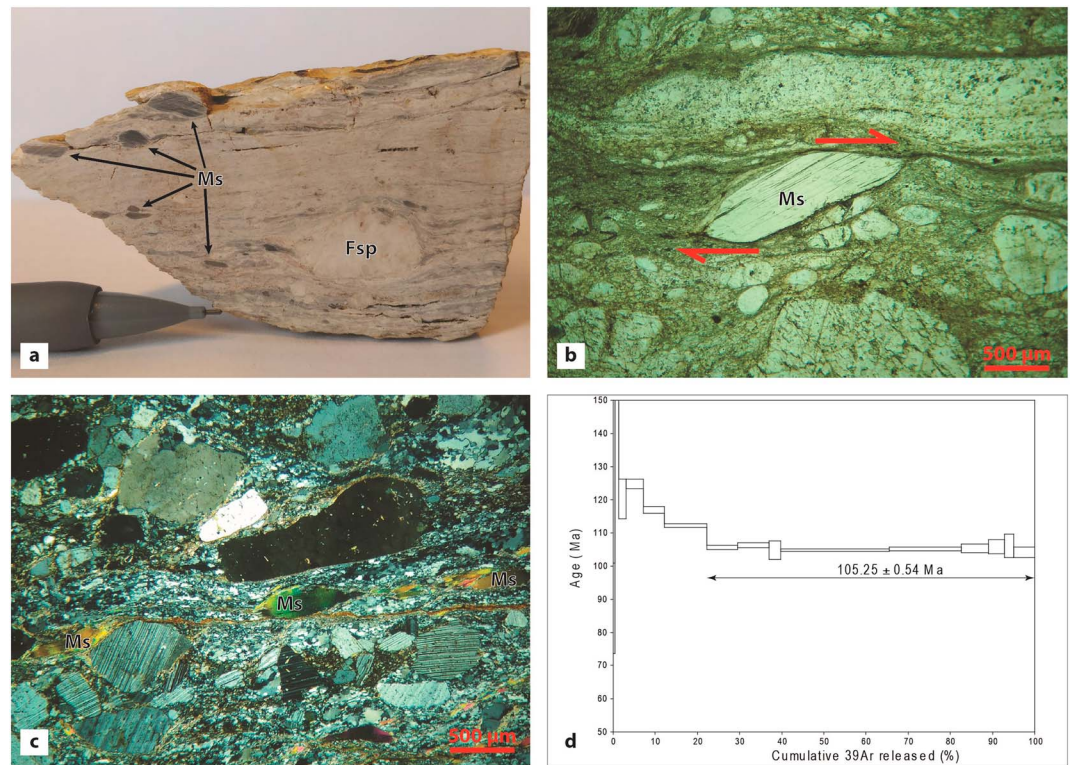


Figure 9. Some characteristics of the leucocratic orthogneiss sample from the southeastern side of the Urdach massif (hill 488) used for $^{40}\text{Ar}/^{39}\text{Ar}$ dating on muscovite (URD 24b). (a) Hand specimen picture. Note millimetric muscovite crystals indicated by black arrows; $^{40}\text{Ar}/^{39}\text{Ar}$ dating was performed on a similar handpicked muscovite crystal. (b) Thin section picture, plane polarized light. (c) Microstructure observed in crossed polarized light. Large muscovite crystals form mica fish and are embedded in a strained recrystallized foliation together with σ -type feldspar porphyroclasts. Shear foliation is defined by recrystallized quartz and mica; quartz recrystallization is dominantly assisted by grain boundary bulging and nucleation (low T fabric). Sense of shear is dextral. (d) ^{39}Ar release spectrum of a handpicked muscovite (see Table 2 for the related data set).

exposed in the Sarailé massif. According to the observed quartz microstructures (Drury & Urai, 1990; Hirth & Tullis, 1992; Law, 2014; Passchier & Trouw, 2005; Stipp et al., 2002) the maximum temperature reached by these rocks during foliation development was of the order of $\sim 400\text{--}450^\circ\text{C}$. As a general observation, in the granitoid rocks exposed in the Urdach massif and in the Urdach Breccia biotite seem to be less chloritized than in the Sarailé massif.

5. Geochronological Data

5.1. $^{40}\text{Ar}/^{39}\text{Ar}$ Dating of a Leptynitic Gneiss (Urdach, URD24b)

During this work, a mylonitic leptynitic gneiss was collected at the Urdach Pass (hill 488, see section 3.2.1) for $^{40}\text{Ar}/^{39}\text{Ar}$ dating (Figure 9). A large single grain of muscovite was analyzed with the laser probe $^{40}\text{Ar}/^{39}\text{Ar}$ step-heating technique using an analytical procedure similar to that described in Clerc et al. (2015). Argon was released on 15 heating steps and 9 of them yield a plateau age of 105.2 ± 0.5 Ma for 78% of the total amount of ^{39}Ar (Figure 9d and Table 2). The first heating steps show evidence of excess argon probably related to the trapping of late ^{40}Ar enriched fluids. Because of a huge radiogenic yield, the isotope correlation plot does not provide a precise value of the initial $^{40}\text{Ar}/^{36}\text{Ar}$ ratio.

The dated muscovite is a large porphyroclast (up to 0.5 mm in diameter), and thus, the meaning of the ~ 105 Ma plateau age has to be discussed considering the conditions of mylonitization. According to microtextural features, temperature is estimated to be in the range $\sim 350\text{--}400^\circ\text{C}$ during deformation, which is below the assumed closure temperature for argon in muscovite (Harrison et al., 2009). For such thermal conditions, and also given its large size, muscovite should have suffered no or only partial resetting during

Table 2
⁴⁰Ar/³⁹Ar Data on Muscovite From Sample URD 24b

Step nb	³⁶ Ar (atm) (fA)	³⁷ Ar (Ca) (fA)	³⁸ Ar (Cl) (fA)	³⁹ Ar (K) (fA)	⁴⁰ Ar (rad) (fA)	Age (Ma)	Error (Ma)	Percent ⁴⁰ Ar (rad)	Percent ³⁹ Ar	
1	0.18231	0.03651	0.09774	0.63588	5.8225	87.27	13.58	9.75	0.51	
2	0.01175	0.00000	0.00000	1.02822	24.6195	219.88	10.46	87.61	0.82	
3	0.33235	0.00000	0.01870	2.20171	28.0410	120.28	5.97	22.21	1.76	
4	0.00552	0.00000	0.00000	5.07211	67.1030	124.78	1.33	97.56	4.07	
5	0.00300	0.00000	0.00000	6.17248	76.4500	117.07	1.02	98.78	4.95	
6	0.00325	0.00000	0.03824	12.54272	148.8023	112.29	0.59	99.28	10.05	
7	0.00372	0.00000	0.01208	9.16205	102.0813	105.65	0.68	98.85	7.34	
8	0.00349	0.12667	0.00000	9,37042	105.0218	106.26	0.72	98.94	7.51	
9	0.00243	0.00000	0.03448	3.43353	37.9562	104.85	2.85	98.06	2.75	
10	0.00631	0.00000	0.00066	32.15598	355.4451	104.84	0.41	99.39	25.77	
11	0.00681	0.00000	0.01135	21.36579	236.9482	105.17	0.53	99.07	17.12	
12	0.00260	0.00000	0.00561	8.02215	89.1251	105.36	1.24	99.06	6.43	
13	0.00163	0.11023	0.00000	4.71259	52.5782	105.79	2.12	99.01	3.78	
14	0.00299	0.00000	0.00000	2.77686	31.0833	106.13	3.56	97.15	2.23	
15	0.00682	0.00000	0.01622	6.11579	67.1935	104.22	1.62	97.00	4.90	
<i>J = 0.005400</i>	<i>Total gas age: 108.53 ± 0.51 Ma</i>						<i>Plateau age: 105.25 ± 0.54 Ma</i>			

mylonitization (Warren et al., 2012), thus providing a plateau age or a staircase age spectrum. Accordingly, the muscovite age at 105 Ma predates the age of deformation that could be responsible for the presence of a loosely bound excess argon component released during the first heating steps on the age spectrum. Leptynitic gneiss analog to the dated sample are found reworked in the late Albian Urdach Breccia, so the mylonitic deformation is well bracketed between ~105 and ~100 Ma. The age of 105 Ma coincides with the age of metasomatic activity all along the Pyrenean belt (i.e., between ~112 and ~92 Ma; e.g., Boutin et al., 2015; Fallourd et al., 2014; Poujol et al., 2010; Schärer et al., 1999) that could have been followed in Urdach by mylonitization some million years later.

6. Discussion: Mode of Thinning of the North Iberia Crustal Basement During Mantle Exhumation

So far, rock samples from the basement of distal passive margin domains were only collected at few localities such as the Iberia-Newfoundland conjugate passive margins, the Bay of Biscay margins, and the southwestern Australian margin, confirming exposures of exhumed lower crust as well as of large areas of serpentinized subcontinental mantle (Beslier et al., 2004; Boillot et al., 1987; Espurt et al., 2012; Péron-Pinvidic & Manatschal, 2009; Tucholke & Sibuet, 2007). Apart from these cases, the basement composition and deformation history of the distal domain of rifted margins remains poorly constrained and highly questionable. Therefore, the geological and geochronological data obtained from the Paleozoic lithologies intimately associated with the Sarailié and Urdach peridotites represent a unique data set providing new parameters to better constrain the processes of extreme crustal thinning and the mechanisms leading to the exposure of subcontinental mantle rocks at distal passive margins in general.

6.1. Implications of Geological Observations and Chronological Data From the Sarailié and Urdach Massifs for the Reconstruction of the Distal Iberian Paleomargin

6.1.1. Temperature and Time Constraints for Crustal Thinning

The large strain that affected the continental crust during its last shearing event is testified by the strongly elongate quartz ribbons found in numerous mylonitic samples. The quartz microstructures reported in section 4 above indicate temperatures in the range of ~300–450 °C for the mylonitic event. All our samples indicate that feldspars deformed brittlely, which indicates that maximum temperatures of deformation did not exceed ~450 °C. In addition, no evidence for a Cretaceous migmatitization has been found during this study nor is this reported in the literature from areas adjacent to the study area. Therefore, we did not find any direct evidence for synextensional partial melting of the continental crust. These observations show that the ductile thinning of the continental crust occurred under greenschist facies conditions. These conditions may correspond either to those characterizing the middle crust, in the case of a stable continental crust with a standard thermal gradient (~30 °C/km), or to those of the upper crust

during a phase of positive thermal anomaly, which resulted in a transient increase of the geothermal gradient.

The greenschist facies mylonitic shearing that we describe in this study may concern andalusite-, amphibole-, or garnet-bearing mica schists, which are typical of amphibolite facies conditions. Thus, this last mylonitic episode has affected metamorphic rocks that originally equilibrated at higher P and T conditions during the Variscan cycle. Interestingly, our sampling set is devoid of rocks deriving from higher grade conditions that might have equilibrated at lower crustal levels such as acidic or basic granulites (kinzigites, charnockites, and pyriclasites). In the western Pyrenees, rocks from this group are easily distinguished and include orthogneisses and paragneisses with garnet, sillimanite, and cordierite in kinzigites and plagioclase and pyroxene in pyriclasites. These rocks are largely exposed in the Ursuya massif to the west of the study area (Boissonnas et al., 1974).

A critical observation from both the Saraillé and Urdach areas is that the long axes of the crustal tectonic lenses as well as their internal foliation always parallel the uppermost boundary of the mantle bodies. In addition, the internal fabric of the crustal lenses parallels the phacoidal fabric of the major detachment zone in the uppermost mantle. This observation strongly suggests that the final fabric of both the continental crust and subcontinental mantle units has been achieved during the same shearing event. The new geochronological data presented in this study have to be combined with the parallel orientation of the crustal mylonitic foliation with the upper limit of the exhumed lherzolite bodies. This demonstrates that the last ductile thinning of the continental crust took place during the Late Albian (105–100 Ma) in relation with subcontinental mantle exhumation. Moreover, the ductile deformation observed at hill 488 is also kinematically consistent with a mylonitic shear zone developed in the lithospheric mantle during its exhumation (750–850 °C and 0.5–1.1 GPa), which is exposed in the Turon de la Técoûère massif, ~10 km to the east in the Chaînons Béarnais (Newman et al., 1999; Vissers et al., 1997).

In the North-Pyrenean Saint-Barthélémy massif (Eastern Pyrenees), Costa and Maluski (1988) reported $^{40}\text{Ar}/^{39}\text{Ar}$ biotite ages of 100–110 Ma for more or less intensely mylonitized rocks at the base of the Trimouns talc quarry. These ages are consistent with the $^{40}\text{Ar}/^{39}\text{Ar}$ age of hydrothermal phlogopite from the alteration rim of a pegmatite (Clerc et al., 2015) as well as with U–Pb ages obtained on minerals related to the talc formation such as monazite, xenotime, rutile, and titanite in the Trimouns talc orebody (Boutin et al., 2015; Schärer et al., 1999). This suggests a genetic relationship between the (re?) activation of shear bands in the thinned Variscan basement of the massif and the penetration and circulation of hydrothermal fluids in its Paleozoic cover. Temperature of mylonitisation in the basement gneiss and granulites is estimated between 400 and 500 °C (Boutin et al., 2015; deSaint Blanquat, 1993), which is well above the temperature needed for the complete argon resetting of Variscan biotite for which a closure temperature of 300–350 °C is assumed (Harrison et al., 1985). These data show that age and temperature of the last mylonitic deformation in the Saint-Barthélémy massif perfectly fit with our estimates for the deformation of the crustal basement exposed in the Urdach and Saraillé massifs.

6.1.2. Overall Deformation Pattern in the Thinned Crust

Field relationships in the Urdach and Saraillé massifs show that the exhumed mantle exposed in the distal domain of the northern Iberian margin was intimately associated with strongly sheared lenses of various crustal lithologies. These lenses display a phacoidal shape with undulating shear contacts between them. The overall pattern of the crustal basement rocks lying over the subcontinental mantle prior to the final stages of its exhumation was represented by a stacking of thin hectometric tectonic lenses. This lenticular mode of deformation allowed the juxtaposition of different lithologies that normally lie at separate levels in the crust, via an anastomosing multidetachment system. The development of multidetachment systems in an extending continental lithosphere is an efficient mechanism to account for the juxtaposition of different crustal layers (e.g., Duretz et al., 2016).

A major information from our petrological study is the abundance of mylonitic continental rocks both in the Urdach Breccia and in the massive units of the Saraillé and Urdach sites. Table 1 displays the proportions of lithological types and strain intensity at both Saraillé and Urdach massifs. At Saraillé, 26 out of 35 samples display a mylonitic to ultramylonitic deformation. At Urdach, 39 out of 56 samples are more or less mylonitized. This leads to an average proportion of 70% of mylonitic samples, which enlightens the relationship between ductile deformed crust and exhumed mantle. This observation cannot be used to quantify precisely the volume of mylonitic rocks in the extended crust welded on the exhumed mantle of the distal

margin domain but indicates that mylonitic deformation has affected a large proportion of the crustal lithologies. A second important information is that this mylonitic deformation did not equally affect the entire crust. Volumes of less deformed material occur in the most internal domains of some of the crustal lenses and often correspond to granitoid plutons and part of their rims of thermal contact metamorphism. These granitoid rocks are reminiscent of those commonly exposed throughout the Axial Zone of the Pyrenees, such as the nearby Eaux-Chaudes and Caunterets plutons. This suggests that the hyperthinned crust that deformed during mantle ascent was not different from the Variscan terranes presently exposed in the unstretched Axial Zone.

It is worth noting that most of the observed mylonitic deformation show evidence for coaxial flattening (e.g., φ -type structures) achieved during pure-shear conditions of deformation, while evidence for a noncoaxial extensional deformation (e.g., sample URD 24b at hill 488) under simple-shear conditions is very rare and localized. This is in agreement with a tectonic scenario during extreme crustal thinning characterized by tectonic lenses with weak internal deformation (i.e., undeformed Paleozoic granitoids) or with purely coaxial flattening, separated by localized noncoaxial ductile shear zones. Such large-scale phacoidal fabric in the extending continental crust have been already imaged by seismic reflection profiles in several regions worldwide, both in the middle crust (e.g., Hamilton, 1987) and in the lower crust (e.g., Reston, 1988) when stretched under pure shear conditions. A scenario with anastomosing mylonitic shear zones separating less deformed internal domains (as the one we describe in this study based on field observations) would explain the peculiar seismic reflectivity of the lower crust observed in some deep-penetration seismic reflection profiles, as already envisaged by Reston (1990).

Crustal rocks exposed in the Urdach massif recorded the transition from ductile to brittle deformation during the Cretaceous rifting. Examples of such transition can be observed at Mer de Her (to the NW of the Urdach massif) or at Soum d'Unars (at the southern tip of the massif), where mylonitic Silurian schists pass to cataclastic breccia cemented by quartz. Similar transitions are frequently observed in isolated breccia clasts at the outcrop scale (Figure 6c) and at the thin section scale, as illustrated in section 4.2. Reworking of various types of mylonite fragments as small clasts as well as large blocks of massive mylonites in the first beds of the Late Albian flysch at Urdach likely results from the denudation and subsequent disaggregation by sedimentary processes of a tectonic breccia. Our mapping shows that the Urdach Breccia lies geologically at the same level as the lenses of massive crustal mylonites, both forming the original cover of the exhumed mantle rocks. This suggests a transition between the massive rocks to the breccia through increasing brittle behavior during extension, which led to the formation of a tectonosedimentary breccia. The shallow dipping shear zones have been progressively exhumed and evolved into cataclastic zones when they reached the brittle field in a way similar to that described by Jolivet et al. (2004, 2010). This process led to a final geometry consisting in boudins of variable size, separated by interboudin necks that pass to exhumed cataclastic breccia.

6.2. Extreme Thinning of the North Iberia Margin in Relation With Mantle Exhumation: A Conceptual Model Based on Geological Observations

Our geological results lead us to define a new configuration for the crust of the North Iberia distal passive margin now inverted in the western NPZ (Figure 10). This configuration, which may vary laterally, is based on the following constraints: (i) post-Silurian Paleozoic rocks are never found in the distal domain; (ii) lower crustal levels did not reach the Earth's surface, at least along the studied paleomargin transect; (iii) extension in the exhumed part of the crust is characterized by lenticular deformation and internal flattening of crustal lenses separated by anastomosing extensional mylonitic shear zones; (iv) at the final step of continental breakup, only crustal lenses derived from pre-Devonian rocks remained welded on the exhumed mantle.

We are well aware that this crustal configuration probably does not apply to all the western north Pyrenean margin for two reasons. (1) Reworked granulitic rocks are reported from the Larau Saint-Engrace Cretaceous formations (Ducasse et al., 1986), to the east of the study area. (2) Lower crustal formations were possibly exposed in the Labourd basement of the Mauléon basin following the Cretaceous extensional episode (Ursuya granulites, Jammes et al., 2009). Therefore, it cannot be excluded that granulites locally reached upper crustal levels during the Cretaceous extension in the western NPZ, such as at Banc Le Danois at the northern margin of the inverted Cantabrian basin (Fügenschuh et al., 2003) and in the Estella Diapir at the SE corner of the basin (Pflug & Schöll, 1976). A lateral segmentation of the North

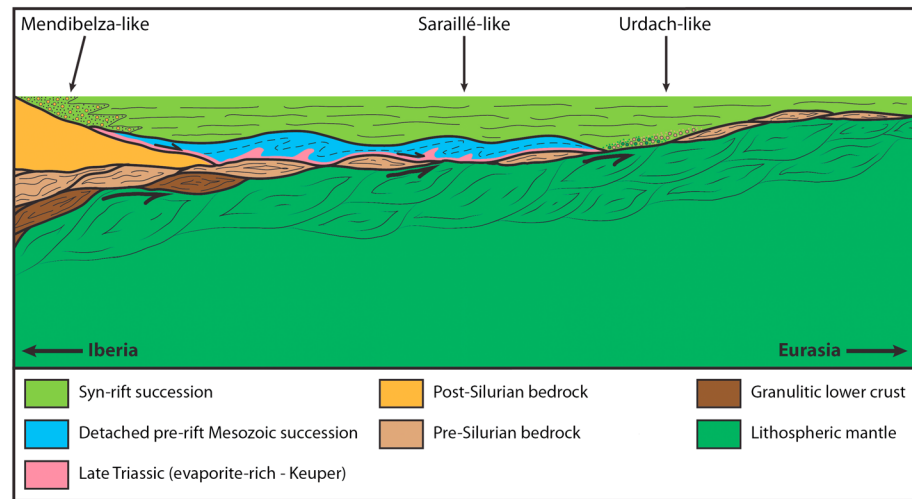


Figure 10. Conceptual reconstruction of the distal domain of the North Iberian paleopassive margin at mid-Cretaceous times as constrained from the data presented in this study. Thin mylonitic pre-Silurian crustal lenses are exhumed together with the mantle at the floor of the Albian-Cenomanian basin; these are locally reworked together in clastic deposits interfingering with the late Albian turbidites (e.g., Urdach Breccia). The granulitic lower crust is extracted laterally and is left behind in the proximal margin domain. The Mesozoic prerift cover glide on a decollement layer represented by the late Triassic evaporites (Keuper) and are locally put in direct contact with the exhumed mantle in the distal domain (e.g., Saraillé massif). Clastic deposits reworking post-Silurian and Mesozoic prerift deposits (e.g., Mendibelza conglomerate) onlap the proximal margin that is simply tilted basinward, without the development of major tilted blocks.

Pyrenean margin has to be considered, as reported from many other margins worldwide. Granulites are also forming the basal crustal levels of some North Pyrenean massifs (e.g., Castillon, Saint Barthelemy, and Agly), but there is no evidence for their exposure to the seafloor during the Mid-Cretaceous although some of them have recorded mylonitic deformation during this time (Costa & Maluski, 1988).

In order to complete the reconstruction of the crustal configuration along a transect representative of the North Iberia margin crust, information on the composition and structure of the proximal margin domain has to be integrated. Critical constraints derive from the geology of the nearby Igountze and Mendibelza units that expose Devonian rocks stratigraphically underlying Mesozoic sediments belonging to the upper margin domain (Masini et al., 2014; Teixell, 1998). During the late Albian extension, syntectonic conglomerates and immature turbidite systems building a few kilometer-wide fan delta system were deposited at the foot of steep slopes of the northern Iberia margin. These deposits, known as the Poudingues de Mendibelza, stratigraphically onlap the Paleozoic formations of the Igountze and Mendibelza massifs composed of thin allochthonous units of late Paleozoic and Mesozoic crustal rocks mainly consisting of Devonian and Carboniferous schists, quartzites and limestones, Permian siltites and conglomerates, Triassic sandstones, and Albian limestones. The composition of the basal chaotic levels (“brèches chaotiques”) of the Mendibelza conglomerate, as well as the unsorted upper levels, directly reflects the nature of their basement. They contain dominantly post-Silurian Paleozoic rocks (Carboniferous schists, quartzites, Devonian limestones, Permian red siltites, and conglomerates) and do not rework deeper levels such as gneisses, granulitoids, mica schists from amphibolite facies conditions, or the granulitic lower crust (Boirie & Souquet, 1982). This indicates that during the Albian extension, the crust of the proximal margin was not dissected by major normal faults able to drive the exhumation of pre-Devonian lithologies. This precludes the development of large fault surfaces such as those required for the formation of upper crustal extensional allochthons, as proposed in alternative reconstruction of the Northern Iberia paleomargin (i.e., Masini et al., 2014).

As discussed in previous works, the peculiar behavior of the Northern Iberia margin during the Cretaceous rifting might have been possible because the necking and distal margin domains have deformed under an almost continuous blanket made of the detached prerift Mesozoic sediments and its overlying Cretaceous flysch cover (Clerc et al., 2015; Clerc & Lagabrielle, 2014; Jammes et al., 2010). Decoupling of the prerift sediments along the Triassic evaporites level is a major feature that allowed crustal deformation under relatively hot conditions (Clerc et al., 2015).

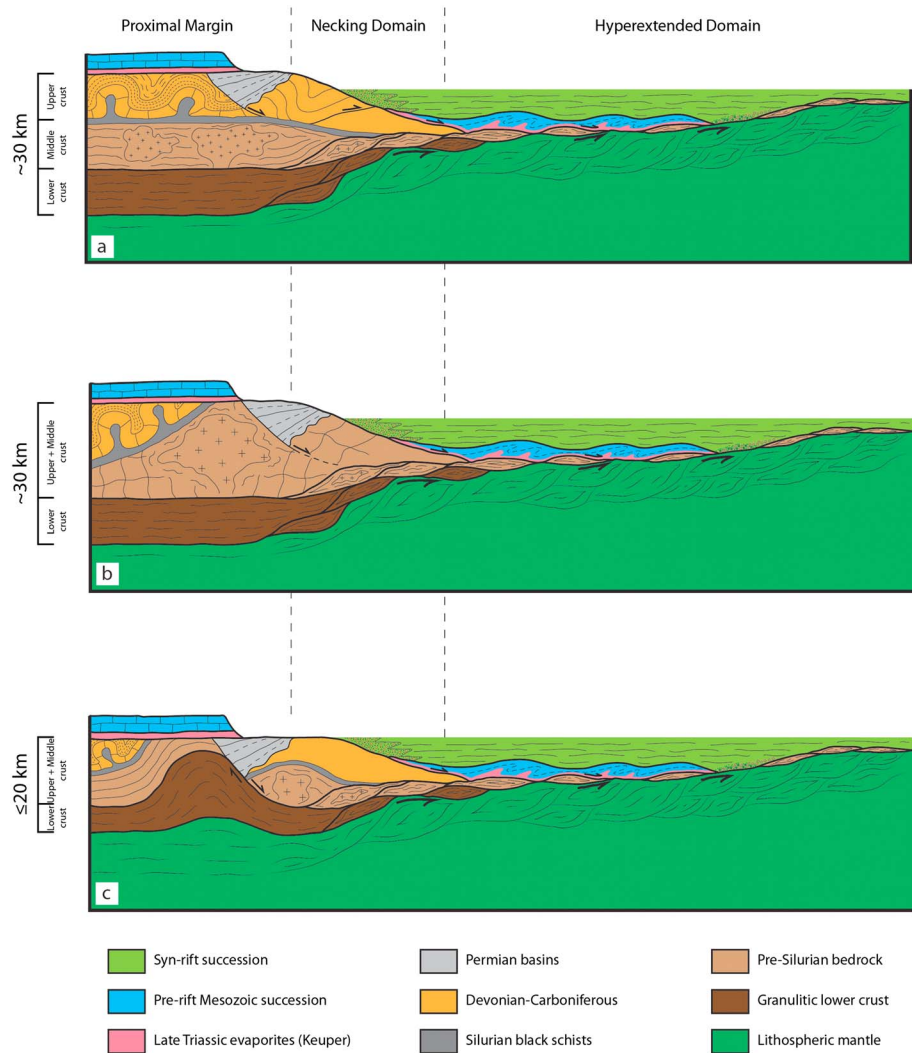


Figure 11. Conceptual reconstruction of the North Iberian paleopassive margin at mid-Cretaceous times as constrained by the data presented in this study with schematic representation of three different hypotheses for the internal structure of the prehyperextended continental crust. For the sake of simplicity, in the proximal domain only pre-Cretaceous structures have been represented. (a) The prehyperextension continental crust has a standard equilibrated thickness (~ 30 km), with the uppermost crust composed of post-Silurian Paleozoic deposits decoupled from the midcrustal pre-Silurian bedrock at the level of the Silurian black schist; in this configuration, the crustal lenses exhumed with the mantle derive from the middle crust. (b) The prehyperextension continental crust has a standard equilibrated thickness (~ 30 km), but with pre-Silurian lithologies already exhumed in some domains and thus representing the upper crust rather than the middle. (c) The prehyperextension continental crust has been already indefinitely thinned during pre-Cretaceous events, with the mantle laying already at depths < 30 km before the Cretaceous. See text (section 6.3) for further explanation.

In our model, the subcontinental mantle, which behaves as a cooling rigid body, is extracted from below a complex of upper/middle crustal tectonic lenses whose basal portion remains welded on the moving mantle. The lower crustal levels are not mobilized probably due to large scale boudinage. Crustal-scale boudinage would explain that rare bodies of lower crust have been locally exhumed to form units such as the Ursuya granulites, to the west of the Mauléon basin. Due to lateral extraction of the ductile part of the crust toward the distal margin domain, the uppermost crust is not dissected by numerous normal faults but is rather tilted basinward, so that the Mendibelza conglomerates progressively onlap the tilted surface exposing mainly Devonian, Carboniferous, and Permo-Triassic rocks. Due to progressive opening of the rift, the decoupled prerift Mesozoic cover remains on top of the deepening axial regions, thus avoiding complete exposure of the exhumed mantle and the ductile crustal lenses to the seafloor. Only some windows, such as in the

Urdach region, have been opened within the detached cover allowing cataclastic crustal units and subcontinental mantle to be directly covered by the first « black flysch » turbidites as early as the Late Albian times.

6.3. Insights on the Prerift Crustal Structure in the Pyrenean Realm

Once the architecture of the distal part of the margin has been reconstructed, an important issue is to determine which were the crustal structure and thickness before the mid-Cretaceous rifting event. As a matter of fact, the starting conditions definitely change the way the continental crust thinned and the significance of the crustal remnants exhumed along with the subcontinental mantle. Considering the available data, there are three reasonable possible pre-Cretaceous configurations as regard to the state of the continental crust (Figure 11): (i) a standard equilibrated thickness (~30 km), with the uppermost crust composed of post-Silurian Paleozoic succession mechanically decoupled from the midcrustal pre-Silurian succession at the level of the Silurian black schist (Figure 11a); (ii) a standard equilibrated thickness (~30 km), but with pre-Silurian lithologies already exhumed in some domains and thus representing the upper crust rather than the middle (Figure 11b); and (iii) an indefinitely prethinned continental crust, with the mantle lying already at depths <30 km before the Cretaceous because of earlier thinning events (Figure 11c).

In the first case, the continental crust would be composed of a lower granulitic layer, a middle crust consisting in the pre-Devonian sequences, and an upper crust consisting of post-Silurian sequences, with the Silurian black schists having an overall horizontal attitude. In this scenario, the Silurian black schists act as an efficient decoupling layer between the upper and the middle crust because of its weak rheological characteristics (Figure 11a). This layer had in fact already acted efficiently as a decollement level during the Variscan orogeny and as rooting layer for the extensional faults controlling the Stephano-Permian basins (e.g., Vissers, 1992; Zwart, 1979). In this case, the ductile crustal lenses exhumed together with the mantle in the study area would represent midcrustal levels exhumed from their original equilibration depth during the mid-Cretaceous rifting. Elision of the granulitic crust mainly results from boudinage of a rigid lower crust, between the subcontinental mantle and the ductile middle crust, and is left behind in the proximal part of the margin. Also the upper crust, comprised between two very efficient decoupling layers (the Silurian schists and the Keuper evaporites), is left behind in the proximal part of the margin.

However, in the Pyrenean domain there is evidence, at least locally, for a pre-Cretaceous exhumation of the pre-Silurian Paleozoic series. Vissers (1992) already proposed the exhumation to the surface of amphibolite facies Paleozoic rocks during a Stephano-Permian denudation phase. As a matter of fact, in the Axial Zone of the central Pyrenees, there is evidence for sedimentary reworking of amphibolite facies Cambro-Ordovician metasediments (de Bresser et al., 1986) and of upper crustal Permian granodioritic intrusions (Nagtegaal, 1969) in Early Triassic conglomerates. Additional evidence comes from the Labourd massif, to the west on the Mauléon basin, where Permo-Triassic sediments unconformably overlay Ordovician (meta)sediments with stratigraphic contacts (Boissonnas et al., 1974), thus demonstrating an early post-Variscan exposure of such lithologies. Considering these constraints, it is possible to propose a second scenario, where all the Paleozoic series and related magmatic intrusions would represent together the upper and middle crust and would behave ductilely as a whole, or at least in its lower portion, below a mobile prerift cover, in the distal part of the margin (Figure 11b). In this hypothesis, too, the granulitic lower crust is boudinaged between the exhuming lithospheric mantle and the ductile upper/middle crust, thus remaining below the proximal part of the margin.

Both models presented above rely on the assumption that the continental crust in the Pyrenees was at standard re-equilibrated conditions before the mid-Cretaceous rifting. However, evidence exists for an early pre-Cretaceous thinning of the continental crust. In the North Pyrenean Massifs there is evidence for a relevant Permian mylonitic extensional event (e.g., Saint Blanquat, 1993; Saint Blanquat et al., 1990), which may have produced up to ~10 km of thinning of the Variscan crust in the Pyrenean realm (Bouhallier et al., 1991). A similar amount of post-Variscan thinning has been proposed by Vissers (1992), who documented the exhumation of amphibolite facies Paleozoic rocks during the aforementioned Stephano-Permian denudation phase that might have accounted for up to 10 km of exhumation. Additional evidence comes from the granulitic units exposed in the NPZ. The lowermost crustal units exposed in outcrop are characterized by low-P granulites which are thought to have equilibrated during Variscan times (Vielzeuf & Kornprobst, 1984) in a range of pressures between 3.5 and 7.5 kbar (e.g., Vielzeuf, 1980, 1984). Crustal rocks that equilibrated at depths ≥ 25 km are thus unknown in the Pyrenean realm. Late Triassic-early Jurassic $^{40}\text{Ar}/^{39}\text{Ar}$ ages on biotite (interpreted as cooling ages below ~300 °C) are documented in the Ursuya massif

granulites, to the west of the Mauléon basin (Masini et al., 2014). Besides, during the whole Mesozoic, especially during the Triassic and the Liassic periods, several episodes of rifting affected the Pyrenean domain (e.g., Debrand-Passard et al., 1995, and references therein) in response to the more or less continuous relative eastward drift of Iberia with respect to Europe and possibly to the dynamics of the opening of the Liguro-Piemontese domain to the east. However, the amount of crustal thinning inherited from these extensional events remains very poorly constrained and might be largely underestimated in our present vision of the crustal structure at the moment of the mid-Cretaceous rifting. All this evidence points to an/some unquantified but likely unneglectable episode(s) of continental crust thinning in the Pyrenean realm before the mid-Cretaceous extensional event, which might have also resulted in a pre-Cretaceous exhumation of the granulitic Variscan lower crust. We can thus envision a third scenario where the Pyrenean crustal thickness did not re-equilibrate after the pre-Cretaceous thinning episode(s), with the granulitic lower crust being locally exhumed (at least partially) and with the subcontinental mantle already lying at depths ≥ 20 km (Figure 11c). In this scenario, the ductile deformation may localize in the entire continental crust in the distal domain. The lithology of the continental units that are exhumed welded on the lithospheric mantle only depends on their position in the crust inherited from prerifting events.

Considering the available data, the third scenario is the most likely. This implies that constraining the crustal structure inherited from previous tectonic events is a fundamental issue to quantify the amount and the style of the Pyrenean Cretaceous lithospheric thinning and definitely deserves further investigation. More in general, determining the role of the inherited crustal structure in the style of lithospheric thinning at diverging plate boundaries is a fundamental issue worldwide. Indeed, attempts to apply general models built from some case studies often fail to account for the structure of other margins, possibly because they neglect differences in the initial conditions inherited from events that precede mantle exhumation.

7. Conclusion

Due to the presence of exceptional exposures deriving from the north Iberia passive margin domains, the western NPZ exemplifies the mechanisms of crustal hyperextension from the microscopic to the regional scale. In this article, we provide several clues issued from a detailed geological survey and the mineralogical study of the two emblematic Sarailé and Urdach massifs that help to better understand the partitioning of the deformation in the continental crust of the North-Iberian margin during hyperextension. Indisputable constraints for the behavior of the distal margin domain preserved in the Chaînons Béarnais during the crustal hyperextension and the ascent of the subcontinental mantle are evidenced and can be summarized as follows: (i) post-Silurian Paleozoic rocks are never found in the distal domain; (ii) extension in the crust is accomplished by lenticular deformation and pervasive ductile flattening through anastomosing extensional mylonitic shear zones at low temperature (350–450 °C maximum); (iii) granulitic rocks are not found in the studied units suggesting early boudinage and lateral extraction of the lower crustal levels; and (iv) at the final step of continental breakup, only pre-Silurian crustal lenses remained welded on the exhumed mantle.

More in general, this study shed light on details of the lithology and structure of the distal part of passive margin that normally lies at abyssal depths. It reveals details of the lithology and structure of distal units that were never reported before. It points to a discrepancy between geological observations from the western Pyrenean analogs and current models of distal margins that can explain some of the differences observed in the first order crustal architectures of many present-day rifted margins. The unique field analog of the Sarailé and Urdach massifs bears a strong potential for the seismic interpretation of hyperextended margins and provides parameters that may constrain the lithologies, the deformation mechanisms, and the strain intensity in units of strongly thinned crust that form significant seismically imaged volumes on some seismic lines from distal margin domains. These new constraints have also to be tested and incorporated into further thermomechanical models for lithospheric stretching and plate separation.

References

- Andersen, T. B., Corfu, F., Labrousse, L., & Osmundsen, P. T. (2012). Evidence for hyperextension along the pre-Caledonian margin of Baltica. *Journal of the Geological Society, London*, 169, 601–612. <https://doi.org/10.1144/0016-76492012-011>
- Beslier, M. O., Royer, J. Y., Girardeau, J., Hill, P. J., Boeuf, E., Buchanan, C., et al. (2004). Une large transition continent-océan en pied de marges sud-ouest australienne: première résultats de la campagne MARGAU/MD110. *Bulletin de la Société Géologique de France*, 175(6), 629–641. <https://doi.org/10.2113/175.6.629>

Acknowledgments

This study is the result of 10 years of research in the NPZ and benefited from grants from various programs that are thoroughly acknowledged here: INSU/Total (PhD thesis of C. Clerc), BRGM/RGF Program (PhD thesis of B. Corre and Master thesis of G. Bergamini), ANR Pyramid and ANR Pyrope, and Total/CNRS-INSU/BRGM Orogen program (postdoctoral grant to R. Asti). This work benefited from insightful and thorough reviews by Tim Reston, Reinoud Vissers, and Franz Neubauer. The authors wish to thank Nicolas Saspiturry for his precious comments and suggestions and for constructive discussions in the field. Y. L. wish to thank especially Loïc Brugalais and Orthofga, Vern/seiche, for making field work possible. All data presented in this manuscript are presented in sections 3–5 or are properly cited and referred to in the reference list.

- Boillot, G., Recq, M., Winterer, E. L., Meyer, A. W., Applegate, J., Baltuck, M., et al. (1987). Tectonic denudation of the upper mantle along passive margins: A model based on drilling results (ODP Leg 103, western Galicia margin, Spain). *Tectonophysics*, *132*(4), 335–342. [https://doi.org/10.1016/0040-1951\(87\)90352-0](https://doi.org/10.1016/0040-1951(87)90352-0)
- Boirie, J.-M., & Souquet, P. (1982). Les poudingues de Mendibelza: Dépôts de cônes sous-marins du rift albien des Pyrénées. *Bulletin des Centres de Recherches Exploration-Production Elf-Aquitaine*, *6*(2), 405–435.
- Boissonnas, J., Destombes, J. P., Heddebaut, C., Le Pochat, G., Lorisignol, S., Roger, P., & Ternet, Y. (1974). In J. Boissonnas, et al. (Eds.), *Carte Géologique France (1/50 000), Feuille Iholdy (1027)* (p. 36). Orléans: BRGM.
- Bouhallier, H., Choukroune, P., & Ballèvre, M. (1991). Evolution structurale de la croûte profonde hercynienne; exemple du massif de l'Agly (Pyrénées orientales, France). *Comptes rendus de l'Académie des sciences Série 2*, *312*, 647–654.
- Boutin, A., de Saint Blanquat, M., Poujol, M., Boulvais, P., Parseval, P., Rouleau, C., & Robert, J. F. (2015). Succession of Permian and Mesozoic metasomatic events in the eastern Pyrenees with emphasis on the Trimouns talc-chlorite deposit. *International Journal of Earth Sciences*, *105*(3), 747–770.
- Canérot, J. (2017). The pull apart-type Tardets-Mauléon Basin, a key to understand the formation of the Pyrenees. *Bulletin Société géologique de France*, *188*(6), 35. <https://doi.org/10.1051/bsgf/2017198>
- Canérot, J., & Delavaux, F. (1986). Tectonic and sedimentation on the north Iberian margin, Chainons Béarnais south Pyrenean zone (Pyrenees basco-béarnaises)—New data about the signification of the lherzolites in the Sarailh area. *Comptes rendus de l'Académie des sciences Série 2*, *302*(15), 951–956.
- Canérot, J., Peybernes, B., & Cizsak, R. (1978). Présence d'une marge méridionale à l'emplacement des Chaînonns Béarnais (Pyrénées basco-béarnaises). *Bulletin de la Société Géologique de France*, *7*(20), 673–676.
- Casteras, M., Canérot, J., Paris, J.-P., Tisin, D., Azambre, B., & Alimen, H. (1970). *Carte géol. France (1/50 000), feuille Oloron-Sainte-Marie (1051)*. Orléans: BRGM.
- Chew, D. M., & van Staal, C. R. (2014). The ocean-continent transition zones along the Appalachian-Caledonian margin of Laurentia: Examples of large-scale hyperextension during the opening of the Iapetus Ocean. *Geoscience Canada*, *41*(2), 165–185. <https://doi.org/10.12789/geocanj.2014.41.040>
- Choukroune, P., & ECORS team (1989). The ECORS Pyrenean deep seismic profile reflection data and the overall structure of an orogenic belt. *Tectonics*, *8*(1), 23–39. <https://doi.org/10.1029/TC008i01p00023>
- Choukroune, P., & Mattauer, M. (1978). Tectonique des plaques et Pyrénées: Sur le fonctionnement de la faille transformante nord-Pyrénéenne; comparaisons avec les modèles actuels. *Bulletin de la Société Géologique de France*, *20*, 689–700.
- Clerc, C., Boulvais, P., Lagabrielle, Y., & de Saint Blanquat, M. (2014). Ophicalcites from the Northern Pyrenean Belt: A field, petrographic and stable isotope study. *International Journal of Earth Sciences*, *103*, 141–163. <https://doi.org/10.1007/s00531-013-0927-z>
- Clerc, C., & Lagabrielle, Y. (2014). Thermal control on the modes of crustal thinning leading to mantle exhumation: Insights from the Cretaceous Pyrenean hot paleomargins. *Tectonics*, *33*, 1340–1359. <https://doi.org/10.1002/2013TC003471>
- Clerc, C., Lagabrielle, Y., Labaume, P., Ringenbach, J.-C., Vauchez, A., Nalpas, T., et al. (2016). Basement—Cover decoupling and progressive exhumation of metamorphic sediments at hot rifted margin. Insights from the Northeastern Pyrenean analog. *Tectonophysics*, *686*, 82–97. <https://doi.org/10.1016/j.tecto.2016.07.022>
- Clerc, C., Lahfid, A., Monié, P., Lagabrielle, Y., Chopin, C., Poujol, M., et al. (2015). High-temperature metamorphism during extreme thinning of the continental crust: A reappraisal of the north Pyrenean passive paleomargin. *Solid Earth*, *6*(2), 643–668. <https://doi.org/10.5194/se-6-643-2015>
- Corre, B., Boulvais, P., Boiron, M. C., Lagabrielle, Y., Marasi, L., & Clerc, C. (2018). Fluid circulations in response to mantle exhumation at the passive margin setting in the north Pyrenean zone, France. *Mineralogy and Petrology*, *112*(5), 647–670. <https://doi.org/10.1007/s00710-018-0559-x>
- Corre, B., Lagabrielle, Y., Labaume, P., Fourcade, S., Clerc, C., & Balleve, M. (2016). Deformation associated with mantle exhumation in a distal, hot passive margin environment: New constraints from the Sarailh Massif (Chainons Béarnais, North-Pyrenean Zone). *Comptes Rendus Geoscience*, *348*(3–4), 279–289. <https://doi.org/10.1016/j.crte.2015.11.007>
- Costa, S., & Maluski, H. (1988). Use of the 40Ar-39Ar stepwise heating method for dating mylonite zones: An example from the St. Barthélémy Massif (Northern Pyrenees, France). *Chemical Geology: Isotope Geoscience*, *72*(2), 127–144. [https://doi.org/10.1016/0168-9622\(88\)90061-9](https://doi.org/10.1016/0168-9622(88)90061-9)
- de Bresser, J. H. P., Majoor, F. J. M., & Ploegsma, M. (1986). New insights in the structural and metamorphic history of the western Lys-Caillaouas massif (Central Pyrenees, France). *Geologie en Mijnbouw*, *65*, 177–187.
- Debrand-Passard, S., et al. coord. (1995). Jurassien. In A. Barnolas & J. C. Chiron (Eds.), *Synthèse géologique et géophysique des Pyrénées*. Édition (Vol. 2, pp. 74–241). Orléans, Madrid: BRGM - ITGE.
- Debroas, E. J., Canérot, J., & Bilotte, M. (2010). Les Brèches d'Urdach, témoins de l'exhumation du manteau pyrénéen dans un escarpement de faille Vraconnien-Cénomaniens inférieur (zone nord-pyrénéenne, Pyrénées-Atlantiques, France). *Géologie de la France*, *2*, 53–63.
- DeFelipe, I., Pedreira, D., Pulgar, J. A., Iriarte, E., & Mendia, M. (2017). Mantle exhumation and metamorphism in the Basque-Cantabrian Basin (N Spain): Stable and clumped isotope analysis in carbonates and comparison with ophicalcites in the North-Pyrenean Zone (Urdach and Lherz). *Geochemistry, Geophysics, Geosystems*, *18*, 631–652. <https://doi.org/10.1002/2016GC006690>
- Deramond, J., Souquet, P., Fondécave-Wallez, M.-J., & Specht, M. (1993). Relationships between thrust tectonics and sequence stratigraphy surfaces in foredeeps: Model and examples from the Pyrenees (Cretaceous-Eocene, France, Spain). In G. D. Williams & A. Dobb (Eds.), *Tectonics and seismic sequence stratigraphy*. Spec. Pub. (Vol. 71, pp. 193–291). London, UK: Geol. Soc. London.
- Drury, M. R., & Urai, J. L. (1990). Deformation related recrystallization processes. *Tectonophysics*, *172*(3–4), 235–253. [https://doi.org/10.1016/0040-1951\(90\)90033-5](https://doi.org/10.1016/0040-1951(90)90033-5)
- Ducasse, L., Vélazque, P. C., & Muller, J. (1986). Glissement de couverture et panneaux basculés dans la région des Arbailles (Pyrénées Occidentales): Un modèle évolutif créacé de la marge nord-Ibérique à l'Est de la transformante de Pamplona. *Comptes rendus de l'Académie des sciences. Série 2*, *303*, 1477–1482.
- Duée, G., Lagabrielle, Y., Coutelle, A., & Fortané, A. (1984). Les lherzolites associées aux Chainons Béarnais (Pyrénées Occidentales): Mise à l'affleurement anté-dogger et résédimentation albo-cénomaniens. *Comptes rendus de l'Académie des sciences. Série 2*, *299*, 1205–1209.
- Duret, T., Petri, B., Mohn, G., Schmalholz, S. M., Schenker, F. L., & Müntener, O. (2016). The importance of structural softening for the evolution and architecture of passive margins. *Nature Scientific Reports*, *6*(1). <https://doi.org/10.1038/srep38704>
- Espurt, N., Callot, J.-P., Roure, F., Totterdell, J. M., Struckmeyer, H. I. M., & Vially, R. (2012). Transition from symmetry to asymmetry during continental rifting: An example from the Bight Basin—Terre Adélie (Australian and Antarctic conjugate margins). *Terra Nova*, *24*(3), 167–180. <https://doi.org/10.1111/j.1365-3121.2011.01055.x>

- Fabriès, J., Lorand, J.-P., & Bodinier, J.-L. (1998). Petrogenetic evolution of orogenic lherzolite massifs in the central and western Pyrenees. *Tectonophysics*, 292, 145–167. [https://doi.org/10.1016/S0040-1951\(98\)00055-9](https://doi.org/10.1016/S0040-1951(98)00055-9)
- Fabriès, J., Lorand, J.-P., Bodinier, J.-L., & Dupuy, C. (1991). Evolution of the upper mantle beneath the Pyrenees: Evidence from orogenic spinel lherzolite massifs. *Journal of Petrology*, 2, 55–76.
- Fallourd, S., Poulou, M., Boulvais, P., Paquette, J. L., de Saint Blanquat, M., & Rémy, P. (2014). In situ LA-ICP-MS U–Pb titanite dating of Na–Ca metasomatism in orogenic belts: The North Pyrenean example. *International Journal of Earth Sciences*, 103(3), 667–682. <https://doi.org/10.1007/s00531-013-0978-1>
- Fortané, A., Duée, G., Lagabrielle, Y., & Coutelle, A. (1986). Lherzolites and the western “Chainons béarnais” (French Pyrénées): Structural and paleogeographical pattern. *Tectonophysics*, 129, 81–98. [https://doi.org/10.1016/0040-1951\(86\)90247-7](https://doi.org/10.1016/0040-1951(86)90247-7)
- Fügensschuh, B., Froitzheim, N., Capdevila, R., & Boillot, G. (2003). Offshore granulites from the Bay of Biscay margins: Fission tracks constrain a Proterozoic to Tertiary thermal history. *Terra Nova*, 15, 337–342. <https://doi.org/10.1046/j.1365-3121.2003.00502.x>
- Gapais, D. (1989). Shear structures within deformed granites: Mechanical and thermal indicators. *Geology*, 17(12), 1144–1147. [https://doi.org/10.1130/0091-7613\(1989\)017<1144:SSWDGM>2.3.CO;2](https://doi.org/10.1130/0091-7613(1989)017<1144:SSWDGM>2.3.CO;2)
- Gaudichet, A. (1974). Etude pétrographique des lherzolites de la région d’Oloron-Ste Marie (Pyrenees Atlantiques). Unpubl. Thesis. Univ. of Paris VI.
- Golberg, J.-M., & Leyrelop, A.-F. (1990). High temperature-low pressure Cretaceous metamorphism related to crustal thinning (Eastern North Pyrenean Zone, France). *Contributions to Mineralogy and Petrology*, 104(2), 194–207. <https://doi.org/10.1007/BF00306443>
- Hamilton, W. (1987). Crustal extension in the Basin and Range Province, southwestern United States. *Geological Society, London, Special Publications*, 28(1), 155–176. <https://doi.org/10.1144/GSL.SP.1987.028.01.12>
- Harrison, T. M., Célérier, J., Aikman, A. B., Hermann, J., & Heizler, M. T. (2009). Diffusion of ⁴⁰Ar in muscovite. *Geochimica et Cosmochimica Acta*, 73(4), 1039–1051. <https://doi.org/10.1016/j.gca.2008.09.038>
- Harrison, T. M., Duncan, I., & McDougall, I. (1985). Diffusion of ⁴⁰Ar in biotite: Temperature, pressure and compositional effects. *Geochimica et Cosmochimica Acta*, 49(11), 2461–2468. [https://doi.org/10.1016/0016-7037\(85\)90246-7](https://doi.org/10.1016/0016-7037(85)90246-7)
- Hirth, G., & Tullis, J. (1992). Dislocation creep regimes in quartz aggregates. *Journal of Structural Geology*, 14(2), 145–159. [https://doi.org/10.1016/0191-8141\(92\)90053-Y](https://doi.org/10.1016/0191-8141(92)90053-Y)
- Jammes, S., Manatschal, G., & Lavier, L. (2010). Interaction between prerift salt and detachment faulting in hyperextended rift systems: The example of the Parentis and Mauléon basins (Bay of Biscay and western Pyrenees). *AAPG Bulletin*, 94(7), 957–975. <https://doi.org/10.1306/12090909116>
- Jammes, S., Manatschal, G., Lavier, L., & Masini, E. (2009). Tectonosedimentary evolution related to extreme crustal thinning ahead of a propagating ocean: Example of the western Pyrenees. *Tectonics*, 28, TC4012. <https://doi.org/10.1029/2008TC002406>
- Jolivet, L., Famin, V., Mehl, C., Parra, T., Aubourg, C., Hébert, R., & Philippot, P. (2004). Strain localization during crustal-scale boudinage to form extensional metamorphic domes in the Aegean Sea. *Geological Society of America Special Papers*, 380, 185–210. <https://doi.org/10.1130/0-8137-2380-9.185>
- Jolivet, L., Labrousse, L., Agard, P., Lacombe, O., Bailly, V., Lecomte, E., et al. (2010). Rifting and shallow-dipping detachments, clues from the Corinth Rift and the Aegean. *Tectonophysics*, 483, 287–304. <https://doi.org/10.1016/j.tecto.2009.11.001>
- Lagabrielle, Y., & Bodinier, J.-L. (2008). Submarine reworking of exhumed subcontinental mantle rocks: Field evidence from the Lherz peridotites, French Pyrenees. *Terra Nova*, 20(1), 11–21. <https://doi.org/10.1111/j.13653121.2007.00781.x>
- Lagabrielle, Y., Clerc, C., Vauchez, A., Lahfid, A., Labaume, P., Azambre, B., et al. (2016). Very high geothermal gradient during mantle exhumation recorded in mylonitic marbles and carbonate breccias from a Mesozoic Pyrenean palaeomargin (Lherz area, North Pyrenean Zone, France). *Comptes Rendus Geosciences*, 348, 257–267.
- Lagabrielle, Y., Labaume, P., & de Saint Blanquat, M. (2010). Mantle exhumation, crustal denudation, and gravity tectonics during Cretaceous rifting in the Pyrenean realm (SW Europe): Insights from the geological setting of the lherzolite bodies. *Tectonics*, 29, TC4012. <https://doi.org/10.1029/2009TC002588>
- Law, R. D. (2014). Deformation thermometry based on quartz c-axis fabrics and recrystallization microstructures: A review. *Journal of Structural Geology*, 66, 129–161. <https://doi.org/10.1016/j.jsg.2014.05.023>
- Le Pichon, X., Bonnin, J., & Sibuet, J. C. (1970). La faille nord-Pyrénéenne: Faille transformante liée à l’ouverture du Golfe de Gascogne. *Comptes Rendus de l’Académie des sciences Série D*, 271, 1941–1944.
- Le Roux, V., Bodinier, J.-L., Tommasi, A., Alard, O., Dautria, J.-M., Vauchez, A., & Riches, A. J. V. (2007). The Lherz spinel lherzolite: Refertilized rather than pristine mantle. *Earth and Planetary Science Letters*, 259(3–4), 599–612. <https://doi.org/10.1016/j.epsl.2007.05.026>
- Masini, E., Manatschal, G., Tugend, J., Mohn, G., & Flament, J. M. (2014). The tectono-sedimentary evolution of a hyper-extended rift basin: The example of the Arzacq–Mauléon rift system (Western Pyrenees, SW France). *International Journal of Earth Sciences*, 103(6), 1569–1596. <https://doi.org/10.1007/s00531-014-1023-8>
- Mohn, G., Manatschal, G., Beltrando, M., Masini, E., & Kuszniir, N. (2012). Necking of continental crust in magma-poor rifted margins: Evidence from the fossil Alpine Tethys margins. *Tectonics*, 31, TC1012. <https://doi.org/10.1029/2011TC002961>
- Monchoux, P. (1970). *Les lherzolites Pyrénéennes: Contribution à l’étude de leur minéralogie, de leur genèse et de leurs transformations*. PhD thesis. Toulouse, France: Univ. of Toulouse.180
- Monchoux, P., Fontan, F., De Parseval, P., Martin, R. F., & Wang, R. C. (2006). Igneous albitite dikes in orogenic lherzolites, western Pyrénées, France: A possible source for corundum and alkali feldspar xenocrysts in basaltic terranes. I. Mineralogical associations. *The Canadian Mineralogist*, 44, 811–836.
- Muñoz, J. A. (1992). Evolution of a continental collision belt: ECORS-Pyrenees crustal balanced cross-section. In K. R. McClay (Ed.), *Thrust Tectonics* (pp. 235–246). London, UK: Chapman and Hall.
- Nagtegaal, P. J. C. (1969). Sedimentology, paleoclimatology, and diagenesis of post-Hercynian continental deposits in the south-central Pyrenees, Spain. *Leidsche Geologische Mededelingen*, 42, 143–238.
- Newman, J., Lamb, W. M., Drury, M. R., & Vissers, R. L. M. (1999). Deformation processes in a peridotite shear zone: Reaction softening by an H₂O-deficient, continuous net transfer reaction. *Tectonophysics*, 303(1–4), 193–222. [https://doi.org/10.1016/S0040-1951\(98\)00259-5](https://doi.org/10.1016/S0040-1951(98)00259-5)
- Nirrengarten, M., Manatschal, G., Tugend, J., Kuszniir, N., & Sauter, D. (2018). Kinematic evolution of the southern North Atlantic: Implications for the formation of hyperextended rift systems. *Tectonics*, 37, 89–118. <https://doi.org/10.1002/2017TC004495>
- Olivet, J. L. (1996). La cinématique de la plaque ibérique. *Bulletin des Centres de Recherches Exploration-Production Elf-Aquitaine*, 20(1), 131–195.
- Passchier, C. W., & Trouw, R. A. J. (2005). *Microtectonics* (366 pp.). Berlin: Springer Verlag.

- Péron-Pinvidic, G., & Manatschal, G. (2009). The final rifting evolution at deep magma-poor passive margins from Iberia-Newfoundland: A new point of view. *International Journal of Earth Sciences*, 98(7), 1581–1597. <https://doi.org/10.1007/s00531-008-0337-9>
- Peron-Pinvidic, G., & Osmundsen, P. T. (2016). Architecture of the distal and outer domains of the mid-Norwegian Vøring rifted margin: Insights from the Rån Ridge system. *Marine and Petroleum Geology*, 77, 280–299. <https://doi.org/10.1016/j.marpetgeo.2016.06.014>
- Pflug, R., & Schöll, W. U. (1976). Un bloque de material jurásico metamorfozado en el Keuper del Diapiro de Estella (Navarra). *Munibe. Sociedad de Ciencias Naturales Aranzadi (San Sebastian)*, 4, 349–353.
- Pin, C., Monchoux, P., Paquette, J.-L., Azambre, B., Wang, R. C., & Martin, R. F. (2006). Igneous albitite dikes in orogenic lherzolites, Western Pyrénées, France: A possible source for corundum and alkali feldspar xenocrysts in basaltic terranes. II. Geochemical and petrogenetic considerations. *The Canadian Mineralogist*, 44, 837–850.
- Pin, C., Paquette, J.-L., Monchoux, P., & Hammouda, T. (2001). First field-scale occurrence of Si–Al–Na-rich low-degree partial melt from the upper mantle. *Geology*, 29(5), 451–454. [https://doi.org/10.1130/0091-7613\(2001\)029<0451:FFSOOS>2.0.CO;2](https://doi.org/10.1130/0091-7613(2001)029<0451:FFSOOS>2.0.CO;2)
- Poujol, M., Boulvais, P., & Kosler, J. (2010). Regional-scale Cretaceous albitization in the Pyrenees: Evidence from in situ U–Th–Pb dating of monazite, titanite and zircon. *Journal of the Geological Society*, 167(4), 751–767. <https://doi.org/10.1144/0016-76492009-144>
- Pryer, L. L. (1993). Microstructures in feldspars from a major crustal thrust zone: The Grenville Front, Ontario, Canada. *Journal of Structural Geology*, 15(1), 21–36. [https://doi.org/10.1016/0191-8141\(93\)90076-M](https://doi.org/10.1016/0191-8141(93)90076-M)
- Puigdefabregas, C., & Souquet, P. (1986). Tectosedimentary cycles and depositional sequences of the Mesozoic and Tertiary from the Pyrenees. *Tectonophysics*, 129, 173–203. [https://doi.org/10.1016/0040-1951\(86\)90251-9](https://doi.org/10.1016/0040-1951(86)90251-9)
- Reston, T. (1988). Evidence for shear zones in the lower crust offshore Britain. *Tectonics*, 7(5), 929–945. <https://doi.org/10.1029/TC007i005p00929>
- Reston, T. (1990). Shear in the lower crust during extension: Not so pure and simple. *Tectonophysics*, 173(1–4), 175–183. [https://doi.org/10.1016/0040-1951\(90\)90215-T](https://doi.org/10.1016/0040-1951(90)90215-T)
- Roure, F., & Choukroune, P. (1998). Contribution of the ECORS seismic data to the Pyrenean geology: Crustal architecture and geodynamic evolution of the Pyrenees. *Mémoires. Société Géologique de France*, 173, 37–52.
- Saint Blanquat, M. (1993). La faille normale ductile du massif du Saint Barthélémy: Evolution hercynienne des massifs nord-pyrénéens catazonaux considérée du point de vue de leur histoire thermique. *Geodinamica Acta*, 6(1), 59–77. <https://doi.org/10.1080/09853111.1993.11105239>
- Saint Blanquat, M., Lardeaux, J. M., & Brunel, M. (1990). Petrological arguments for high-temperature extensional deformation in the Pyrenean Variscan crust (Saint Barthélémy Massif, Ariège, France). *Tectonophysics*, 177(1–3), 245–262. [https://doi.org/10.1016/0040-1951\(90\)90284-F](https://doi.org/10.1016/0040-1951(90)90284-F)
- Salardon, R., Carpentier, C., Bellahsen, N., Pironon, J., & France-Lanord, C. (2017). Interactions between tectonics and fluid circulations in an inverted hyper-extended basin: Example of Mesozoic carbonate rocks of the western North Pyrenean Zone (Chainons Béarnais, France). *Marine and Petroleum Geology*, 80, 563–586. <https://doi.org/10.1016/j.marpetgeo.2016.11.018>
- Schärer, U., de Parseval, P., Polvé, M., & St Blanquat, M. (1999). Formation of the Trimouns talc-chlorite deposit (Pyrenees) from persistent hydrothermal activity between 112 and 97 Ma. *Terra Nova*, 11(1), 30–37. <https://doi.org/10.1046/j.13653121.1999.00224.x>
- Sibuet, J.-C., Srivastava, S. P., & Spakman, W. (2004). Pyrenean orogeny and plate kinematics. *Journal of Geophysical Research*, 109, B08104. <https://doi.org/10.1029/2003JB002514>
- Srivastava, S. P., Sibuet, J. C., Cande, S., Roest, W. R., & Reid, I. D. (2000). Magnetic evidence for slow seafloor spreading during the formation of the Newfoundland and Iberian margins. *Earth and Planetary Science Letters*, 182(1), 61–76. [https://doi.org/10.1016/S0012-821X\(00\)00231-4](https://doi.org/10.1016/S0012-821X(00)00231-4)
- Stipp, M., Stunitz, H., Heilbronner, R., & Schmid, S. M. (2002). The eastern Tonale fault zone: A “natural laboratory” for crystal plastic deformation for quartz over a temperature range from 250 to 700 °C. *Journal of Structural Geology*, 24(12), 1861–1884. [https://doi.org/10.1016/S0191-8141\(02\)00035-4](https://doi.org/10.1016/S0191-8141(02)00035-4)
- Teixell, A. (1998). Crustal structure and orogenic material budget in the west central Pyrenees. *Tectonics*, 17(3), 395–406. <https://doi.org/10.1029/98TC00561>
- Teixell, A., Labaume, P., Ayarza, P., Espurt, N., de Saint Blanquat, M., & Lagabrielle, Y. (2018). Crustal structure and evolution of the Pyrenean-Cantabrian belt: A review and new interpretations from recent concepts and data. *Tectonophysics*, 724–725, 146–170.
- Teixell, A., Labaume, P., & Lagabrielle, Y. (2016). The crustal evolution of the west-central Pyrenees revisited: Inferences from a new kinematic scenario. *Comptes Rendus Géoscience*, 348(3–4), 257–267. <https://doi.org/10.1016/j.crte.2015.10.010>
- Thiébaud, J., Durand-Wackenheim, C., Debeaux, M., & Souquet, P. (1992). Métamorphisme des évaporites triasiques du versant nord des Pyrénées centrales et Occidentales. *Bulletin de la Société d'histoire naturelle de Toulouse*, 128, 77–84.
- Tucholke, B. E., & Sibuet, J.-C. (2007). Leg 210 synthesis: Tectonic, magmatic, and sedimentary evolution of the Newfoundland-Iberia rift. In B. E. Tucholke, J.-C. Sibuet, & A. Klaus (Eds.), *Proceedings of the Ocean Drilling Program, Scientific Results* (Vol. 210, pp. 1–56). College Station, TX: Ocean Drilling Program. <https://doi.org/10.2973/odp.proc.sr.210.101.2007>
- Tugend, J., Manatschal, G., Kuszniir, N. J., Masini, E., Mohn, G., & Thionon, I. (2014). Formation and deformation of hyperextended rift systems: Insights from rift domain mapping in the Bay of Biscay-Pyrenees. *Tectonics*, 33, 1239–1276. <https://doi.org/10.1002/2014TC003529>
- Vergés, J., & Garcia-Senz, J. (2001). Mesozoic evolution and Cainozoic inversion of the Pyrenean rift. In P. A. Ziegler, et al. (Eds.), *Peri-Tethys Memoir 6: Peri-Tethyan rift/wrench basins and passive margins. Mémoires du Muséum national d'histoire naturelle* (Vol. 186, pp. 187–212). Paris, France: Muséum national d'histoire naturelle.
- Vielzeuf, D. (1980). Pétrologie des écaillés granulitiques de la région de Lherz (Ariège). Thèse de 3ème cycle, Clermont-Ferrand.
- Vielzeuf, D. (1984). Relations de phases dans le faciès granulite et implications géodynamiques. L'exemple des granulites des pyrénées. Thèse, Clermont-Ferrand.
- Vielzeuf, D., & Kornprobst, J. (1984). Crustal splitting and the emplacement of Pyrenean lherzolites and granulites. *Earth and Planetary Science Letters*, 67(1), 87–96. [https://doi.org/10.1016/0012-821X\(84\)90041-4](https://doi.org/10.1016/0012-821X(84)90041-4)
- Vissers, R. L. M. (1992). Variscan extension in the Pyrenees. *Tectonics*, 11(6), 1369–1384. <https://doi.org/10.1029/92TC00823>
- Vissers, R. L. M., Drury, M. R., Newman, J., & Fliervoet, T. F. (1997). Mylonitic deformation in upper mantle peridotites of the North Pyrenean Zone (S France): Implications for strength and strain localization in the lithosphere. *Tectonophysics*, 279(1–4), 303–325. [https://doi.org/10.1016/S0040-1951\(97\)00128-5](https://doi.org/10.1016/S0040-1951(97)00128-5)
- Vissers, R. L. M., & Meijer, P. T. (2012). Mesozoic rotation of Iberia: Subduction in the Pyrenees? *Earth-Science Reviews*, 110(1–4), 93–110. <https://doi.org/10.1016/j.earscirev.2011.11.001>
- Warren, C. J., Hanke, F., & Kelly, S. P. (2012). When can muscovite ⁴⁰Ar/³⁹Ar dating constrain the timing of metamorphic exhumation? *Chemical Geology*, 291, 79–86. <https://doi.org/10.1016/j.chemgeo.2011.09.017>

- Whitney, D. L., & Evans, B. W. (2010). Abbreviations for names of rock-forming minerals. *American Mineralogist*, 95(1), 185–187. <https://doi.org/10.2138/am.2010.3371>
- Wrobel-Daveau, J.-C., Ringenbach, J.-C., Tavakoli, S., Ruiz, G. M. H., Masse, P., & Frizon de Lamotte, D. (2010). Evidence for mantle exhumation along the Arabian margin in the Zagros (Kermanshah area, Iran). *Arabian Journal of Geosciences*, 3(4), 499–513. <https://doi.org/10.1007/s12517-010-0209-z>
- Zwart, H. J. (1979). The geology of the central Pyrenees. *Leidse Geologische Mededelingen*, 50, 1–74.